

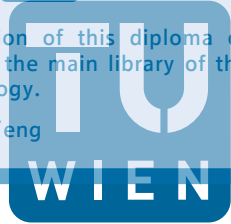
Die approbierte Originalversion dieser Diplom-/
Masterarbeit ist in der Hauptbibliothek der Tech-
nischen Universität Wien aufgestellt und zugänglich.

<http://www.ub.tuwien.ac.at>



The approved original version of this diploma or
master thesis is available at the main library of the
Vienna University of Technology.

<http://www.ub.tuwien.ac.at/eng>



TECHNISCHE
UNIVERSITÄT
WIEN

Vienna University of Technology

DIPLOMARBEIT

Description of a Bottle Resonator Evanescently Coupled to a Waveguide

Ausgeführt am Institut für
Theoretische Physik
der Technischen Universität Wien

unter der Anleitung von
Univ.-Prof. Stefan Rotter

durch

Bernhard Schlederer

Gerichtsgasse 1/17/32
A-1210 Wien

Datum

Unterschrift

Contents

1	Introduction	5
2	Coupling between the Waveguide and the Bottle Resonator	7
2.1	Modes of the Isolated Structures	7
2.1.1	Modes of the Waveguide	7
2.1.2	Modes of the Bottle Resonator	10
2.2	Coupled Mode Theory	14
2.2.1	Preliminary Considerations	15
2.2.2	Coupled Mode Equations	17
2.2.3	Conservation of Energy Flux	19
2.2.4	Properties of the Propagation Matrix	20
2.3	Sample Calculations for Optical Conveyor Belt	21
3	Scattering Matrix Models	25
3.1	Two-Mode Model	25
3.1.1	Basic Equations of the Model	26
3.1.2	Decay Time	29
3.1.3	Solution of the Equations	31
3.1.4	Exemplary Spectra	33
3.2	Four-Mode Model	37
3.2.1	Basic Equations of the Model	37
3.2.2	Solutions of the Equations	42
3.2.3	Transmissions and Reflections	44
3.2.4	Exemplary Spectra	46
4	Non-Hermitian Hamiltonian Model	51
4.1	Introduction	51
4.2	Connection to Four-Mode Model	53
4.2.1	Eigenmodes of the Non-Hermitian Hamiltonian and the Four-Mode Model	54
4.2.2	Linking Both Models	55
4.3	No Energy Creation	57
4.3.1	Time Evolution	57
4.3.2	Condition for Model Parameters	58

4.3.3 Chirality and Frequency Splitting Quality	61
5 Preliminary Experimental Data and Chiral Modes	63
5.1 Transmission and Reflection	63
5.2 Chirality and Frequency Splitting Quality	67
6 Four Dimensional Scattering Matrix for Left-Right-Symmetric Systems	69
7 Summary and Outlook	75
Bibliography	77

1 Introduction

Optical microresonators are widely used in numerous applications, such as for filtering and switching in optical communications, biochemical sensing, microlasers and cavity quantum electrodynamics [1, 2]. The ratio of quality factor and volume Q/V is important for these applications because this figure describes how long and how strongly the confined light interacts coherently with matter (e.g. with single atoms). To this day the highest values for Q/V have been reached with whispering-gallery-modes in microresonators, like the bottle microresonator investigated here [1–3].

In contrast to other microresonators, for example microspheres or -disks, it is possible to tune the resonance frequencies of the bottle microresonator by more than half or their free spectral range by applying a longitudinal stress. This is important because the resonator can thus be set to be at resonance for any given frequency. Furthermore the whispering-gallery-modes exhibit two so-called caustics where the intensity of the light is significantly increased which can be used to couple light in and out through an ultra-thin fiber [1, 2].

Although many interesting phenomena have already been studied with bottle resonators, their interaction with fibers has only been described heuristically so far. In this thesis we will introduce a more solid theoretical framework by using a coupled mode theory to compute the coupling between an ultra-thin waveguide and the resonator which we will also apply to a concrete problem. Most importantly, this will also provide the basis for the development of the models described in later chapters.

We will first be concerned with describing the fundamental mode of a waveguide and with finding approximate expressions for the resonator modes. In a next step, we will approximate the field in the coupling region, where the fiber and the resonator approach each other closely, by a superposition of both aforementioned modes. By demanding that the reciprocity theorem shall also hold for this superposition, the so-called coupled mode equations will be derived. These linear differential equations yield a propagation matrix that connects incoming and outgoing mode amplitudes. Using the coupled mode theory, we will also be able to address the experimentally relevant question whether a so-called nanofiber-based conveyor belt can work near a bottle resonator. We will see that the so-called phase-matching between fiber and resonator modes plays a crucial part for this problem.

In a next step, based on the work with the coupled mode theory, we will develop

models which aim to properly describe the transmission and reflection spectra of our bottle resonator-waveguide system. Scattering matrices will be used to model the interaction between the different modes under consideration. The coupling region of the fiber and the resonator will be modelled by means of the propagation matrix mentioned above. It will always be assumed that the fiber is sufficiently far apart from the bottle resonator such that the coupling is adiabatic, i.e. that no backscattering or dissipation occurs in the coupling region. First, a simple model that only includes dissipation in the resonator, but no scattering, will be described to introduce some basic ideas for this simpler setting. In a next step this model will be extended to also account for scattering between the two counterpropagating resonator modes. For both cases explicit formulas for the amplitudes of all the modes involved will be given. Furthermore, conditions which ensure that the energy flux in the bottle resonator is conserved, or at least can only be dissipated, will be deduced.

Subsequently, we will make use of a non-hermitian model introduced in [4–6] to describe open-systems, similar to our bottle resonator. The most interesting part about this model is that it allows for so-called "chiral modes" to occur which have so far not been experimentally demonstrated. By the term "chiral modes" we mean a nearly-degenerate mode pair where both modes, in contrast to strictly-degenerate ones in closed systems, exhibit the same sense of rotation inside the cavity. This is possible due to the fact that the model describes the interaction between the counterpropagating modes of the bottle resonator by way of a non-hermitian Hamiltonian. Our aim will be to investigate how this model is accordable with the ones previously described and which implications the occurrence of chiral modes have, especially regarding transmission and reflection spectra. Going beyond the stationary regime, we will also investigate the time evolution of the bottle resonator modes following this approach. By demanding that no energy shall be created within the resonator, we will derive a condition for the model parameters. This will be our main finding, allowing us to quantitatively describe under which circumstances chiral modes can occur.

Finally, we will present preliminary experimental data kindly provided by our colleagues from the group of Arno Rauschenbeutel to compare the predictions of the previously described models with actual measurements. As we will see, the results are quite promising and indicate the existence of chiral modes in the bottle resonator although further investigation will still be needed to rule out other explanations and to show if the effects are reproducible.

2 Coupling between the Waveguide and the Bottle Resonator

First of all, it should be noted that, since the author's diploma thesis is the continuation of his previous "Projektarbeit" [7], major parts of this chapter have been taken from there in order to make this work self-contained.

2.1 Modes of the Isolated Structures

In this section we will establish exact expressions for the modes of the waveguide and approximate ones for the bottle resonator. This is necessary because they are needed for the coupled mode theory we will describe afterwards.

2.1.1 Modes of the Waveguide

First, we will look into the modes of a cylindrical waveguide whose cross-section is shown in Fig. 2.1. To obtain the corresponding modes one has to solve Maxwell's equations for dielectrics with a relative permittivity ε_r that describes the different material in the optical fiber.

$$\varepsilon_r = \begin{cases} n_{co}^2, & 0 \leq \rho \leq r_{wg} \\ n_{cl}^2, & r_{wg} < \rho < \infty \end{cases} \quad \text{with} \quad \begin{pmatrix} x \\ y \end{pmatrix} = \begin{pmatrix} \rho \cos(\phi) \\ \rho \sin(\phi) \end{pmatrix} \quad (2.1)$$

Here the constants n_{co} and n_{cl} shall be the refractive indices of the core and the cladding of the waveguide respectively and r_{wg} shall be the radius of the core. Note that the cladding could as well be air or vacuum as will be assumed later on. As can be seen in Fig. 2.1 the z -axis has been chosen to lie in the axial direction.

As is well known, a Helmholtz equation for any of the two regions with constant refractive index can be derived from Maxwell's equations

$$\left(\nabla^2 + n^2 \frac{\omega^2}{c^2} \right) \vec{\Psi}(\rho, \phi, z) = 0 \quad \text{with} \quad \vec{\Psi} = \vec{E}, \vec{H}. \quad (2.2)$$

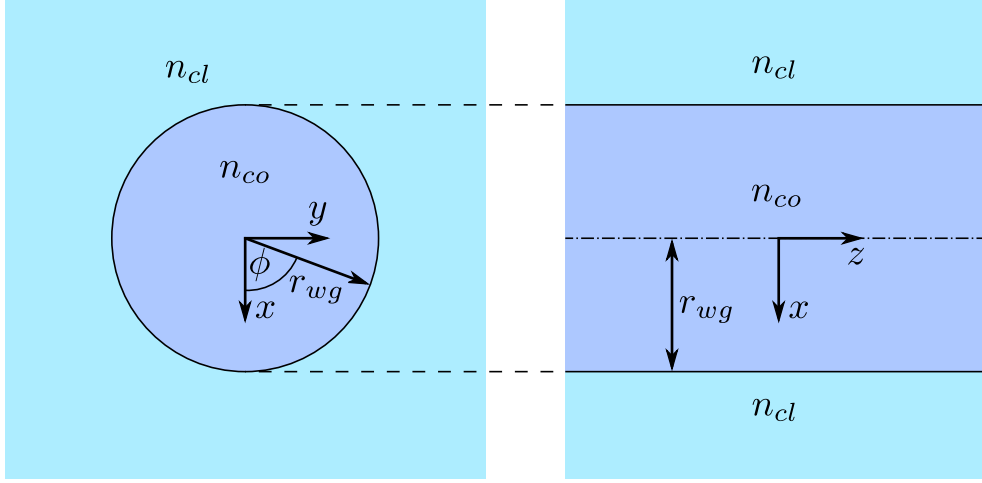


Figure 2.1: Cross-section and top view of the waveguide.

The constant c denotes the speed of light and n equals n_{co} or n_{cl} when inside the core or the cladding, respectively. Here we have also introduced that the time dependence of the electromagnetic field shall be of the form $e^{i\omega t}$ with angular frequency ω .

Moreover, the electric field \vec{E} and the magnetic field \vec{H} have to satisfy the interface conditions for electromagnetic fields. In our case the magnetic field has to be continuous because no currents are present and the permeability is constant. Likewise, the azimuthal- and the z -component of the electric field also have to be continuous. On the other hand, the radial component of the electric field, which is normal to the interface, has to satisfy

$$\lim_{\rho \rightarrow r_{wg}^-} n_{co}^2 E_\rho(\rho) = \lim_{\rho \rightarrow r_{wg}^+} n_{cl}^2 E_\rho(\rho). \quad (2.3)$$

Since we are only interested in modes that travel in the axial direction, i.e. the z -direction, the z -dependence of the modes has to be of the form

$$\vec{E}(\rho, \phi, z) = \vec{e}(\rho, \phi) e^{-i\beta z} \quad \text{and} \quad \vec{H}(\rho, \phi, z) = \vec{h}(\rho, \phi) e^{-i\beta z} \quad (2.4)$$

where β is the so-called propagation constant. The functions \vec{e} and \vec{h} describe the profile of the electric and magnetic field in the xy -plane, respectively. By inserting this into the previous wave equation we see that the z -components e_z and h_z of the electric and magnetic field profiles have to obey

$$\left(\frac{1}{\rho} \partial_\rho (\rho \partial_\rho) + \frac{1}{\rho^2} \partial_\phi^2 - \beta^2 + n_{co}^2 k^2 \right) \psi = 0, \quad 0 \leq \rho < r_{wg} \quad (2.5)$$

$$\left(\frac{1}{\rho} \partial_\rho (\rho \partial_\rho) + \frac{1}{\rho^2} \partial_\phi^2 - \beta^2 + n_{cl}^2 k^2 \right) \psi = 0, \quad r_{wg} < \rho < \infty \quad (2.6)$$

where $k = \frac{\omega}{c}$ is the vacuum wave number and ψ stands for e_z and h_z . By means of a separation ansatz the equations (2.5) and (2.6) can be rewritten into Bessel's differential equation whose solutions are well known. Additionally taking into account that the interface conditions must hold, expressions for the z -components of the electromagnetic field can be obtained. The other components can be deduced by inserting the z -components into Maxwell's equations and solving for the remaining ones.

Due to the interface conditions only a discrete set of modes exists for a given frequency ω and waveguide radius r_{wg} , which can be classified into HE, EH, TE and TM modes. The general solutions for all those types will not be given here because only the fundamental mode HE_{11} will be needed in the following. The expressions for the other modes and a much more detailed version of the outlined derivation here can be found in references [8–10]. Pictures of the intensity distributions of the different modes are shown in [9, 10].

Since, in this work, we are only interested in ultra-thin optical fibers whose radii are so small that no higher-order modes exist, we can restrict ourselves to the fundamental mode HE_{11} of the waveguide. Note that the "cladding" of the ultra-thin waveguide is the air or the vacuum around it and therefore $n_{cl} = 1$.

The field components in cylindrical coordinates of the HE_{11} mode inside the fiber ($\rho < r_{wg}$) are given by [8]

$$\begin{aligned} e_r &= -\frac{a_1 J_0(UR) + a_2 J_2(UR)}{J_1(U)} f(\phi), & h_r &= \sqrt{\frac{\varepsilon_0}{\mu_0}} \frac{k n_{co}^2}{\beta} \frac{a_3 J_0(UR) - a_4 J_2(UR)}{J_1(U)} g(\phi) \\ e_\phi &= -\frac{a_1 J_0(UR) - a_2 J_2(UR)}{J_1(U)} g(\phi), & h_\phi &= -\sqrt{\frac{\varepsilon_0}{\mu_0}} \frac{k n_{co}^2}{\beta} \frac{a_3 J_0(UR) + a_4 J_2(UR)}{J_1(U)} f(\phi) \\ e_z &= i \frac{U}{r_{wg} \beta} \frac{J_1(UR)}{J_1(U)} f(\phi), & h_z &= i \sqrt{\frac{\varepsilon_0}{\mu_0}} \frac{U F_2}{r_{wg} k} \frac{J_1(UR)}{J_1(U)} g(\phi) \end{aligned} \quad (2.7)$$

and the field components outside the fiber ($\rho > r_{wg}$) are given by

$$\begin{aligned} e_r &= -\frac{U}{W} \frac{a_1 K_0(WR) - a_2 K_2(WR)}{K_1(W)} f(\phi), & h_r &= \sqrt{\frac{\varepsilon_0}{\mu_0}} \frac{U}{W} \frac{k n_{co}^2}{\beta} \frac{a_5 K_0(WR) + a_6 K_2(WR)}{K_1(W)} g(\phi) \\ e_\phi &= -\frac{U}{W} \frac{a_1 K_0(WR) + a_2 K_2(WR)}{K_1(W)} g(\phi), & h_\phi &= -\sqrt{\frac{\varepsilon_0}{\mu_0}} \frac{U}{W} \frac{k n_{co}^2}{\beta} \frac{a_5 K_0(WR) - a_6 K_2(WR)}{K_1(W)} f(\phi) \\ e_z &= i \frac{U}{r_{wg} \beta} \frac{K_1(WR)}{K_1(W)} f(\phi), & h_z &= i \sqrt{\frac{\varepsilon_0}{\mu_0}} \frac{U F_2}{r_{wg} k} \frac{K_1(WR)}{K_1(W)} g(\phi) \end{aligned} \quad (2.8)$$

where the abbreviations

$$R = \frac{\rho}{r_{wg}}, \quad \Delta = \frac{1}{2} \left(1 - \frac{n_{cl}^2}{n_{co}^2} \right), \quad (2.9)$$

$$f(\phi) = \begin{cases} \cos(\phi) \\ \sin(\phi) \end{cases}, \quad g(\phi) = \begin{cases} -\sin(\phi) \\ \cos(\phi) \end{cases} \quad \begin{array}{l} \text{for even modes} \\ \text{for odd modes} \end{array} \quad (2.10)$$

$$\begin{aligned}
V &= r_{wg} k \sqrt{n_{co}^2 - n_{cl}^2}, \quad U = r_{wg} \sqrt{k^2 n_{co}^2 - \beta^2}, \quad W = r_{wg} \sqrt{\beta^2 - k^2 n_{cl}^2}, \\
b_1 &= \frac{1}{2U} \left(\frac{J_0(U)}{J_1(U)} - \frac{J_2(U)}{J_1(U)} \right), \quad b_2 = -\frac{1}{2W} \left(\frac{K_0(W)}{K_1(W)} + \frac{K_2(W)}{K_1(W)} \right), \\
F_1 &= \left(\frac{UW}{V} \right)^2 (b_1 + (1 - 2\Delta)b_2), \quad F_2 = \left(\frac{V}{UW} \right)^2 \frac{1}{b_1 + b_2}, \\
a_1 &= \frac{F_2 - 1}{2}, \quad a_3 = \frac{F_1 - 1}{2}, \quad a_5 = \frac{F_1 - 1 + 2\Delta}{2}, \\
a_2 &= \frac{F_2 + 1}{2}, \quad a_4 = \frac{F_1 + 1}{2}, \quad a_6 = \frac{F_1 + 1 - 2\Delta}{2}
\end{aligned} \tag{2.11}$$

were used. The permittivity and permeability in vacuum is denoted by ε_0 and μ_0 . The functions J_ν and K_ν are the ν -th Bessel function of the first kind and the ν -th modified Bessel function of the second kind, respectively.

The propagation constant β is given by the equation [8]

$$k^2 n_{co}^2 F_1 = \beta^2 F_2 \tag{2.12}$$

that arises from the interface conditions. Equation (2.12) has to be solved by numerical means because F_1 and F_2 also depend on β . The propagation constant β always lies within the range of $k n_{cl} < \beta < k n_{co}$, which is useful when searching for the value of β that solves above equation.

As long as V in (2.11) is smaller than 2.405... (i.e. the first root of the zeroth Bessel function of the first kind J_0) the waveguide remains in single-mode operation because then only the fundamental HE_{11} mode exists. By looking at the definition of V in (2.11) it is clear that mono-mode operation appears for decreasing r_{wg} or decreasing k .

2.1.2 Modes of the Bottle Resonator

The Glass Cylinder

Next, we will describe the modes of the bottle resonator for which we have to deal with the whispering gallery modes of a glass cylinder first. This is necessary because the resonator modes will be approximated by a modulation of these along the axial direction. The glass cylinder can be thought of as the waveguide depicted in Fig. 2.1 where air (or vacuum) is used as its "cladding", i.e. $n_{cl} = 1$. As before, we have chosen that the z -axis shall lie in the axial direction.

Once again, a wave equation for the electric and magnetic field can be derived from Maxwell's equations for dielectrics. The differential equation for the z -components of the field (E_z and H_z) in cylindrical coordinates has the form

$$\left(\frac{1}{\rho} \partial_\rho (\rho \partial_\rho) + \frac{1}{\rho^2} \partial_\phi^2 + \partial_z^2 + n^2 k^2 \right) \psi(\rho, \phi, z) = 0 \text{ with } \psi = E_z, H_z \tag{2.13}$$

where k is the vacuum wave number. The refractive index n has the value of the refractive index of silica $n_{sil} \approx 1.47$ when inside the glass cylinder and equals one outside the glass. Moreover, the electromagnetic field has to satisfy the same interface conditions as the step-profile fiber before and the time dependence of the fields shall again be of the form $e^{i\omega t}$ with angular frequency ω .

Unlike before, we are now interested in modes that rotate around the axis of the glass cylinder and do not travel along the z -direction. Thus we stipulate that the desired solutions of equation (2.13) shall be independent of z and have a ϕ -dependence of the form $e^{-im\phi}$, where the azimuthal wave number m has to be an integer ($\phi = 0$ and $\phi = 2\pi$ have to yield the same result). Using these assumptions equation (2.13) changes to

$$\left(\frac{1}{\rho}\partial_{\rho}(\rho\partial_{\rho}) - \frac{m^2}{\rho^2} + n^2k^2\right)\psi(\rho, \phi) = 0 \quad (2.14)$$

which can be rewritten as Bessel's differential equation. Solving equation (2.14) yields the z -components of the electromagnetic field of the whispering gallery modes

$$\psi(\rho, \phi) = \begin{cases} \frac{J_m(n_{sil} k \rho)}{J_m(n_{sil} k r_0)} e^{-im\phi}, & 0 \leq \rho < r_0 \\ \frac{Y_m(k \rho)}{Y_m(k r_0)} e^{-im\phi}, & r_0 < \rho < \infty \end{cases} \quad (2.15)$$

where the continuity of the z -components has already been taken into account. The radius of the cylinder is denoted by r_0 and the functions J_m and Y_m are the m -th Bessel function of the first and second kind, respectively. The other field components can be expressed by inserting E_z or H_z into Maxwell's equations, which yields:

$$\begin{aligned} E_{\rho}(\rho, \phi) &= -\frac{m}{\rho \omega \varepsilon_0 n^2} H_z(\rho, \phi) \\ E_{\phi}(\rho, \phi) &= \frac{i}{\omega \varepsilon_0 n^2} \partial_{\rho} H_z(\rho, \phi) \\ H_{\rho}(\rho, \phi) &= \frac{m}{\rho \omega \mu_0} E_z(\rho, \phi) \\ H_{\phi}(\rho, \phi) &= -\frac{i}{\omega \mu_0} \partial_{\rho} E_z(\rho, \phi) \end{aligned} \quad (2.16)$$

Two different types of solutions can be distinguished which are named TM and TE modes. For TE (TM) polarisation E_z (H_z) is set equal to zero which, because of (2.16), also forces the field components H_{ρ} and H_{ϕ} (E_{ρ} and E_{ϕ}) to be zero. The z -component H_z (E_z) for TE (TM) polarisation is obtained from (2.15) and the remaining components E_{ρ} and E_{ϕ} (H_{ρ} and H_{ϕ}) are determined through (2.16).

For every azimuthal wave number m only a discrete set of frequencies ω (or equivalently wave numbers k) are permitted that are determined due to the interface conditions which can be written as:

$$\frac{n_{sil} J'_m(n_{sil} k r_0)}{J_m(n_{sil} k r_0)} = \frac{Y'_m(k r_0)}{Y_m(k r_0)} \text{ for TM modes} \quad (2.17)$$

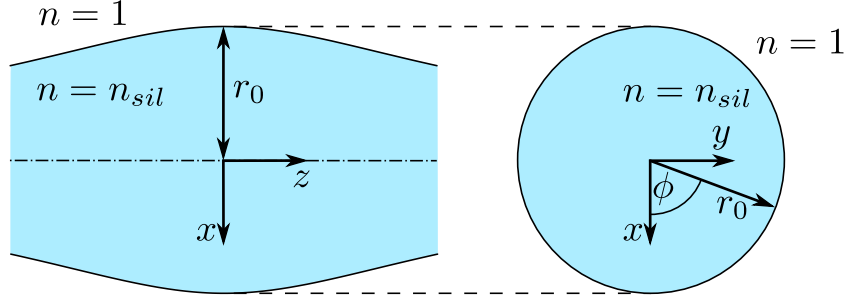


Figure 2.2: Cross-section and top view of the bottle resonator. Note that the curvature of the bottle resonator along the z -axis is exaggerated for better visibility.

$$\frac{J'_m(n_{sil} k r_0)}{J_m(n_{sil} k r_0)} = \frac{n_{sil} Y'_m(k r_0)}{Y_m(k r_0)} \text{ for TE modes} \quad (2.18)$$

Here, only the solution with the lowest frequency (i.e. k), for a given m , is of interest since it corresponds to a mode that is mostly located at the outer rim of the glass cylinder and is therefore best suited for coupling purposes. Such modes are called whispering gallery modes. Note that one has to find the lowest wave number k_m of equation (2.17) or (2.18) only once for any given azimuthal wave number m (and refractive index n_{sil}) and some radius r_0 . After defining $\alpha_m = k_m r_0$ the wave number for any other radius (but for the same m and n_{sil}) can easily be calculated from α_m .

The Bottle Resonator

After obtaining an exact solution for the modes of the glass cylinder we can now investigate the modes of the bottle resonator. To get an idea of the shape of the bottle resonator and to see how the coordinate system has been chosen, cross-sections are shown in Fig. 2.2. We again use the wave equation for the z -components of the electromagnetic field E_z and H_z

$$(\nabla^2 + n^2 k^2) \Psi(\rho, \phi, z) = 0 \text{ with } \Psi = E_z, H_z \quad (2.19)$$

where a time dependence of the form $e^{i\omega t}$ has been assumed. As previously, k and n denote the vacuum wave number and the refractive index, respectively. In contrast to the glass cylinder, the radius of the bottle resonator $r(z)$ shall now slowly vary along the z -direction

$$r(z) = \frac{r_0}{\sqrt{1 + (\Delta k z)^2}} \quad (2.20)$$

with a maximal radius of r_0 at $z = 0$. We assume that the curvature Δk shall be small (i.e. $\Delta k r_0 \ll 1$). Note that n now not only depends on ρ but also on z (although it still remains piecewise constant).

To obtain an approximate solution we use the following ansatz [11, 12]

$$\Psi = Z(z) \psi_{m,r(z),p}(\rho, \phi) \quad (2.21)$$

where $\psi_{m,r(z),p}$ shall denote either the z -component of the electric or the magnetic field¹ of the glass cylinder mode (see (2.15)) with azimuthal wave number m and radius $r(z)$ and polarization p . Consequently, Ψ only stands for the z -component of either the electric or the magnetic field.²

To determine the function $Z(z)$ we insert the above ansatz for Ψ into equation (2.19) and arrive at

$$Z''(z) + n^2 \left(k^2 - \frac{\alpha_m^2}{r(z)^2} \right) Z(z) = 0 \quad (2.22)$$

where we neglected all z -derivatives of $\psi_{m,r(z),p}$ since $r(z)$ shall only vary slowly along the z -axis.³ The constant α_m was obtained from solving (2.17) or (2.18), depending on the polarization p . Note that n is not a constant in (2.22) but depends on ρ and z , i.e. it equals n_{sil} inside and one outside the glass. However, the function $Z(z)$ can only satisfy equation (2.22) for one value of n . Since the mode of the glass cylinder is much more located inside the glass the value $n = n_{sil}$ should approximate the problem more accurately and will be used in the following.

After inserting $r(z)$ into (2.22) we obtain

$$-Z''(z) + v_m^2 z^2 Z(z) = E Z(z) \text{ with } v_m = n_{sil} \Delta k \frac{\alpha_m}{r_0}, E = n_{sil}^2 \left(k^2 - \frac{\alpha_m^2}{r_0^2} \right) \quad (2.23)$$

which resembles the differential equation of a harmonic oscillator. Thus the solutions of (2.23) are given by [11, 12]

$$Z_{q,m}(z) = H_q(\sqrt{v_m} z) e^{-v_m \frac{z^2}{2}} \quad (2.24)$$

with eigenvalues

$$E_{q,m} = 2 v_m \left(q + \frac{1}{2} \right) \quad (2.25)$$

where H_q denotes the q -th Hermite polynomial. The axial wave number q has to be an integer and counts the nodes of H_q and $Z_{q,m}$. Since $E_{q,m}$ in (2.25) also equals

$$E_{q,m} = n_{sil}^2 \left(k_{q,m}^2 - \frac{\alpha_m^2}{r_0^2} \right) \quad (2.26)$$

¹ It is electric if $p = \text{TM}$ and magnetic if $p = \text{TE}$, cf. the paragraph after (2.16).

² It is electric if $p = \text{TM}$ and magnetic if $p = \text{TE}$, cf. the paragraph after (2.16).

³ This is also referred to as the adiabatic approximation.

per definition from (2.23), one can calculate the approximate vacuum wave number $k_{q,m}$ (or equivalently the resonance frequency $\omega_{q,m}$) of the whispering gallery modes for any azimuthal and axial wave number,⁴

$$k_{q,m} = \sqrt{\frac{\alpha_m^2}{r_0^2} + \frac{2 \alpha_m \Delta k}{n_{sil} r_0} \left(q + \frac{1}{2} \right)}. \quad (2.27)$$

Note that the form of $Z_{q,m}$ in (2.24) gives rise to two regions with enhanced intensity, the so-called caustics, which are approximately located at $\pm \alpha_m / k_{q,m}$.

Until now, we have only obtained one z -component of the electromagnetic field, i.e. $H_z = \Psi$ ($E_z = \Psi$) if the polarization p equals TM (TE). In a similar way as described in the paragraph below (2.16) the other z -component is set equal to zero. The ρ - and ϕ -components of the electromagnetic field are obtained by inserting the z -components into the equations (2.16). Be aware, however, that the expressions for the modes of the bottle resonator obtained here are only approximations to the real field distribution and exactly fulfil Maxwell's equations only at the caustic, where $Z(z)$ has its maximum [11].

For further reading, pictures of the modes and more detailed versions of the above derivation of the bottle resonator modes we refer to the references [3, 11, 12]. That the axial field distribution is indeed approximately described by (2.24) was experimentally confirmed by exciting erbium doped bottle resonators (see Fig. 1 in [1]). For more experimental details, possible future applications and how the bottle resonators can be manufactured from glass fibers the reader shall be referred to [2].

2.2 Coupled Mode Theory

At the beginning of this section, it will be explained which modes of the fiber and the bottle resonator couple efficiently to each other. In a next step, the electromagnetic field of the waveguide plus the resonator will be approximated by a linear combination of those modes within the framework of a coupled mode theory [13–15]. By demanding that the reciprocity theorem, which can be derived from Maxwell's equation, shall also hold for the approximated field, a set of differential equations, the so-called coupled mode equations, will be derived. Since the coupled mode equations are linear differential equations, they give rise to a propagation matrix, that connects incoming and outgoing amplitudes. Subsequently, we will show that the coupled mode equations conserve the energy flux and that the propagation matrix must be unitary and symmetric. At the end of this section, a simplified formula for calculating the coupling strength between a mode of the fiber and a mode of the resonator, that couple efficiently, will be derived.

⁴ and polarization p since α_m depends on it

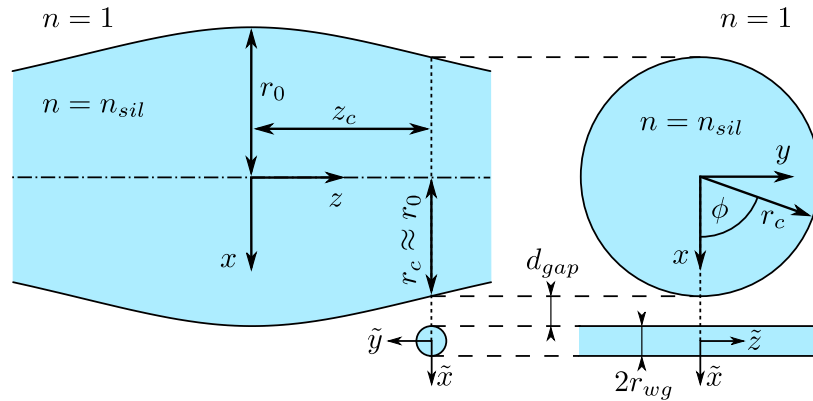


Figure 2.3: Cross-section and top view of the combined system of the bottle resonator and the fiber. Note that the curvature of the bottle resonator and the radius of the fiber are exaggerated for better visibility.

For a general theoretical background of the coupled mode theory see e.g. references [16–19]. See, in addition, [20, 21] and page 376 of [14] for further information about the validity of the coupled mode theory in different settings.

2.2.1 Preliminary Considerations

In contrast to the section before we are not dealing with isolated dielectric structures anymore but with coupled devices, as shown in Fig. 2.3. The origin of the coordinate system chosen for the composite structure shall lie on the axis in the middle of the bottle resonator where the radius has its maximum. The z -axis shall point into the axial direction of the bottle resonator and the y -axis shall be parallel to the waveguide. Additionally a coordinate system for the waveguide shall be introduced as depicted in Fig. 2.3. Its origin shall lie on the axis of the fiber where it passes the resonator. The \tilde{z} -axis shall point into the axial direction of the waveguide and the \tilde{x} -axis shall be parallel to the x -axis.⁵

In order to excite a bottle resonator mode with the evanescent field of an ultra-thin optical fiber, the frequency of the waveguide mode has to coincide with the resonance frequency. Additionally, as stated on page 100 in [11], the waveguide and the resonator mode have to travel into the same direction,⁶ must spatially overlap with each other and have the same polarization. To meet the second condition, the waveguide has to be located where the bottle resonator mode, that shall be

⁵ The transformation between the two coordinate systems is as follows: $x = \tilde{x} + r_c$, $y = \tilde{z}$ and $z = -\tilde{y} + z_c$.

⁶ For example when the resonator mode rotates counterclockwise around the z -direction, i.e. it has a time and ϕ -dependence of the form $e^{i(\omega t - m\phi)}$, the fiber mode must travel into the positive y -direction.

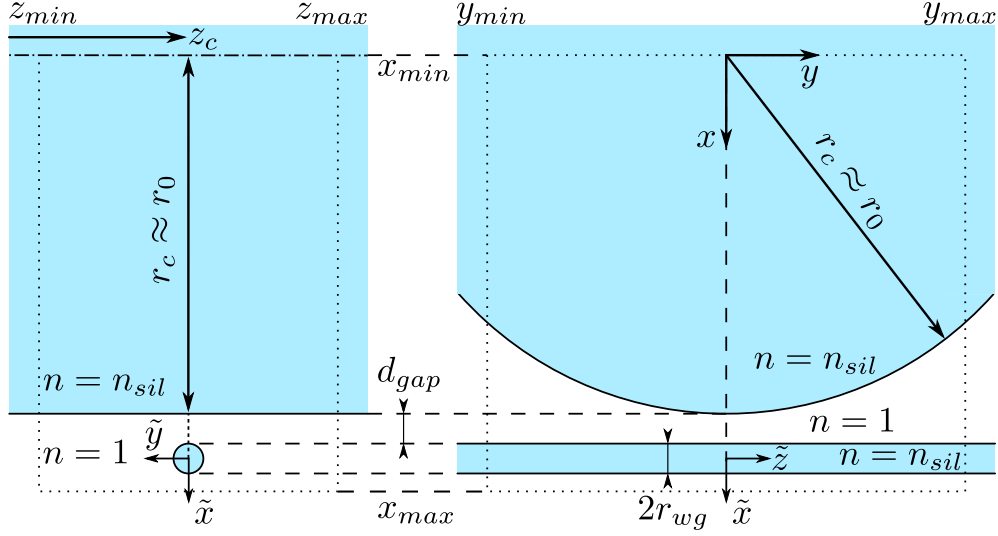


Figure 2.4: Cross-section and top view of the combined system of the bottle resonator and the fiber with emphasis of the computational window (boundaries indicated by dotted lines). Note that, since the curvature of the bottle resonator shall be small, the radius of the resonator has been approximated to be constant within the computational window. As in Fig. 2.3, the fiber radius is exaggerated.

excited, has its caustic, i.e. where it has maximal intensity. Consequently, if the gap between the fiber and the resonator increases or if the fiber is not exactly located at the caustic, the coupling decreases. The last condition means that the waveguide mode must have an odd polarization to excite the TM modes of the resonator or an even polarization for TE modes.⁷

The coupled mode theory we are going to employ was adopted from [13–15]. For the implementation of the coupled mode theory only the domain, where the overlap between the waveguide and resonator mode is significant, is considered. This domain, also called computational window, is indicated by dotted lines in Fig. 2.4. Note that since the problem here (in contrast to [13–15]) is three-dimensional, the computational window also has to be of three dimensions. The position and sizes of the window have to be chosen to cover the domain where the fiber gets close to the resonator, i.e. where the coupling is non-negligible. The domain of the computational window used for the calculations performed for this work was

$$x \in [x_{min} = 0, x_{max} = r_0 + d_{gap} + 5r_{wg}], y \in [y_{min} = -\frac{3}{4}r_{wg}, y_{max} = \frac{3}{4}r_{wg}] \quad (2.28)$$

$$\text{and } z \in [z_{min} = z_c - 10r_{wg}, z_{max} = z_c + 10r_{wg}]$$

⁷ The polarization of the resonator (the waveguide) is meant to be realized for the coordinate system in Fig. 2.3 without (with) the tilde.

where z_c shall be the position of the caustic of the bottle resonator mode under investigation (it is assumed that the waveguide is also located there, cf. Fig. 2.3). The parameter d_{gap} shall denote the gap between the fiber and the resonator (see Fig. 2.3 or Fig. 2.4) and is in the range of the radius of the waveguide r_{wg} . For comparison, the radius of the waveguide r_{wg} is usually about 50 to 100 times smaller than the radius of the bottle resonator at its maximal value r_0 . The radius r_c of the bottle resonator at z_c , i.e. at the caustic, is almost identical to r_0 due to the resonator's small curvature. Typical values for r_{wg} are hundreds of nanometers and r_0 should at least be 15 μm to reduce radiative losses [1]. The computational window has to be chosen large enough such that a larger one would yield no significant difference in the results. This has been checked for the above mentioned window for all sets of parameters (i.e. radii, curvature, etc.) used in this work.

2.2.2 Coupled Mode Equations

To describe the coupling of a bottle resonator mode $\{\vec{E}_r, \vec{H}_r\}$ with the waveguide mode $\{\vec{E}_w, \vec{H}_w\}$ that couples efficiently to it, the field of the composite structure $\{\vec{E}, \vec{H}\}$ in the computational window will be approximated as a y -dependent linear combination of both fields, i.e.

$$\vec{E}(\vec{r}) = a_i(y)\vec{E}_i(\vec{r}) \text{ and } \vec{H}(\vec{r}) = a_i(y)\vec{H}_i(\vec{r}) \text{ with } i = r, w \quad (2.29)$$

where Einstein's summation convention has been used. Be aware that this approximation has an inherent flaw since the waveguide mode does not fulfil the interface conditions of the resonator structure and vice versa. Therefore the approximation is better for larger than for smaller distances between the fiber and the resonator. For more details see [20, 21] and page 376 of [14]. In accordance with the requirement of efficient coupling both fields must have the same frequency ω and thus the same time dependence $e^{i\omega t}$. For the following equations we will assume that the relative permittivity is constant and equal to one in the entire space since we are describing silica.

In order to determine the functions $a_i(y)$ we demand that the reciprocity theorem

$$\begin{aligned} \int \vec{\nabla} \cdot (\vec{E}_j \times \vec{H}_i^* + \vec{E}_i^* \times \vec{H}_j) dx dz &= \partial_y \int \vec{e}_y \cdot (\vec{E}_j \times \vec{H}_i^* + \vec{E}_i^* \times \vec{H}_j) dx dz = \\ &= -i\omega\epsilon_0 \int \vec{E}_i^* \cdot (\epsilon_j - \epsilon_i)\vec{E}_j dx dz \text{ with } i, j = r, w \end{aligned} \quad (2.30)$$

which holds for any two solutions of Maxwell's equations, shall also hold for $\{\vec{E}, \vec{H}\}$, i.e.

$$\partial_y \int \vec{e}_y \cdot (\vec{E} \times \vec{H}_i^* + \vec{E}_i^* \times \vec{H}) dx dz = -i\omega\epsilon_0 \int \vec{E}_i^* \cdot (\epsilon - \epsilon_i)\vec{E} dx dz. \quad (2.31)$$

The relative permeability ε_r (ε_w) shall only describe the dielectric structure of the resonator (the waveguide) without the waveguide (the resonator) and ε shall be the permeability distribution of the composite dielectric structure, i.e. the bottle resonator plus the optical fiber.

After inserting the ansatz given in (2.29) for the electromagnetic field $\{\vec{E}, \vec{H}\}$ into (2.31) one obtains

$$\begin{aligned}
& \partial_y \int \vec{e}_y \cdot \left(\vec{E} \times \vec{H}_i^* + \vec{E}_i^* \times \vec{H} \right) dx dz = \tag{2.32} \\
& = \partial_y \int a_j(y) \vec{e}_y \cdot \left(\vec{E}_j \times \vec{H}_i^* + \vec{E}_i^* \times \vec{H}_j \right) dx dz = \\
& = a'_j(y) \int \vec{e}_y \cdot \left(\vec{E}_j \times \vec{H}_i^* + \vec{E}_i^* \times \vec{H}_j \right) dx dz + \\
& + a_j(y) \partial_y \int \vec{e}_y \cdot \left(\vec{E}_j \times \vec{H}_i^* + \vec{E}_i^* \times \vec{H}_j \right) dx dz = \\
& = a'_j(y) \int \vec{e}_y \cdot \left(\vec{E}_j \times \vec{H}_i^* + \vec{E}_i^* \times \vec{H}_j \right) dx dz + \\
& + a_j(y) \left(-i\omega\varepsilon_0 \int \vec{E}_i^* \cdot (\varepsilon_j - \varepsilon_i) \vec{E}_j dx dz \right) =
\end{aligned}$$

for the left hand side and

$$= -i\omega\varepsilon_0 \int \vec{E}_i^* \cdot (\varepsilon - \varepsilon_i) \vec{E} dx dz = -i\omega\varepsilon_0 a_j(y) \int \vec{E}_i^* \cdot (\varepsilon - \varepsilon_i) \vec{E}_j dx dz$$

for the right hand side. Note that we have derived two equations at the same time, one for $i = r$ and one for $i = w$.

The above equations can be rewritten as

$$\begin{pmatrix} \sigma_{rr} & \sigma_{rw} \\ \sigma_{wr} & \sigma_{ww} \end{pmatrix} \begin{pmatrix} a'_r(y) \\ a'_w(y) \end{pmatrix} = \begin{pmatrix} c_{rr} & c_{rw} \\ c_{wr} & c_{ww} \end{pmatrix} \begin{pmatrix} a_r(y) \\ a_w(y) \end{pmatrix} \tag{2.33}$$

where the abbreviations

$$\sigma_{ij}(y) = \int \vec{e}_y \cdot \left(\vec{E}_j \times \vec{H}_i^* + \vec{E}_i^* \times \vec{H}_j \right) dx dz \tag{2.34}$$

$$c_{ij}(y) = -i\omega\varepsilon_0 \int \vec{E}_i^* \cdot (\varepsilon - \varepsilon_j) \vec{E}_j dx dz \tag{2.35}$$

have been used. Note that the domain of integration in (2.34) and (2.35) is the computational window.⁸ The system of linear differential equations in (2.33) are

⁸ An exception is σ_{rr} where the integration has to be taken over the whole z -axis because the overlap of the resonator mode with itself is mostly not located within the computational window.

called coupled mode equations. It can be easily seen that $\sigma_{ij} = \sigma_{ji}^*$ by looking at the definition in (2.34). Moreover, since our problem has a left-right symmetry, which is evident from Fig. 2.4, it is simple to show that $\sigma_{ij}(-y) = \sigma_{ij}^*(y)$ and $c_{ij}(-y) = -c_{ij}^*(y)$.

From the coupled mode equations a propagation matrix T

$$\begin{pmatrix} a_r(y_{max}) \\ a_w(y_{max}) \end{pmatrix} = \begin{pmatrix} T_{rr} & T_{rw} \\ T_{wr} & T_{ww} \end{pmatrix} \begin{pmatrix} a_r(y_{min}) \\ a_w(y_{min}) \end{pmatrix} \quad (2.36)$$

can be obtained, due to the linearity of the problem, that connects the amplitudes of the outgoing modes (at y_{max}) of the resonator and the waveguide with the incoming ones (at y_{min}). Solving the coupled mode equations with the initial condition $a_r(y_{min}) = 1$ and $a_w(y_{min}) = 0$ for the functions $a_r(y)$ and $a_w(y)$ yields the matrix elements

$$T_{rr} = a_r(y)|_{y=y_{max}} \text{ and } T_{wr} = a_w(y)|_{y=y_{max}}. \quad (2.37)$$

The matrix elements T_{rw} and T_{ww} can be obtained in a similar manner when using the initial condition $a_r(y_{min}) = 0$ and $a_w(y_{min}) = 1$.

2.2.3 Conservation of Energy Flux

An interesting property of the coupled mode formulation is that it conserves the energy flux through the xz -plane for different y -coordinates. The energy flux through such a plane is given by its two dimensional integral of the Poynting vector \vec{S} projected onto the normal vector \vec{e}_y of the plane. In the following we are going to calculate the y -derivative of this integral, i.e.

$$\begin{aligned} \partial_y \int \vec{e}_y \cdot \vec{S} \, dx \, dz &\propto \partial_y \int \vec{e}_y \cdot \left(\vec{E} \times \vec{H}^* + \vec{E}^* \times \vec{H} \right) \, dx \, dz = \quad (2.38) \\ &= \partial_y \int a_j(y) a_i^*(y) \vec{e}_y \cdot \left(\vec{E}_j \times \vec{H}_i^* + \vec{E}_i^* \times \vec{H}_j \right) \, dx \, dz = \\ &= a_i^* \sigma_{ij} a_j' + a_i'^* \sigma_{ij} a_j + a_i^* a_j \left(-i\omega \varepsilon_0 \int \vec{E}_i^* \cdot (\varepsilon_j - \varepsilon_i) \vec{E}_j \, dx \, dz \right) = \\ &= -i\omega \varepsilon_0 a_i^* a_j \left(\int \vec{E}_i^* \cdot (\varepsilon - \varepsilon_j) \vec{E}_j \, dx \, dz - \right. \\ &\quad \left. - \int \vec{E}_i^* \cdot (\varepsilon - \varepsilon_i) \vec{E}_j \, dx \, dz + \int \vec{E}_i^* \cdot (\varepsilon_j - \varepsilon_i) \vec{E}_j \, dx \, dz \right) = 0 \end{aligned}$$

with $\vec{S} \propto \vec{E} \times \vec{H}^* + \vec{E}^* \times \vec{H}$, $\sigma_{ij} a_j' = c_{ij} a_j$ and $a_i'^* \sigma_{ij} = \sigma_{ji}^* a_i'^* = c_{ji}^* a_i^*$

Equation (2.38) yields zero and thus shows that the energy flux through the xz -plane is independent of y and therefore conserved.

2.2.4 Properties of the Propagation Matrix

Unitarity of the Propagation Matrix

As can easily be seen when looking at the definition in (2.34) σ_{rr} and σ_{ww} are proportional to the integral of the Poynting vector \vec{S} over the xz -plane. Thus they are also proportional to the energy flux of the resonator or the fiber mode respectively. Note that, since solutions of Maxwell's equations must conserve the energy flux, σ_{rr} and σ_{ww} must be independent of the position y they are evaluated. Assuming that the fields of the waveguide and the resonator at the boundary of the computational window (i.e. at y_{min} and y_{max}) are far enough apart such that they do no longer overlap, i.e.

$$\int \vec{e}_y \cdot \left(\vec{E}_j \times \vec{H}_i^* + \vec{E}_i^* \times \vec{H}_j \right) dx dz \approx 0 \text{ for } j \neq i \quad (2.39)$$

the energy flux at the positions y_{min} and y_{max} is proportional to

$$|a_r(y)|^2 \sigma_{rr} + |a_w(y)|^2 \sigma_{ww} \text{ for } y = y_{min}, y_{max} \quad (2.40)$$

If the modes are normalized such that $\sigma_{rr} = 1$ and $\sigma_{ww} = 1$, energy flux conservation is given by

$$|a_r(y_{min})|^2 + |a_w(y_{min})|^2 = |a_r(y_{max})|^2 + |a_w(y_{max})|^2 \quad (2.41)$$

In order for the last equation to hold for every pair of incoming amplitudes the propagation matrix T has to be unitary.

Symmetry of the Propagation Matrix

Assuming that we already obtained a solution $a_j(y)$ for the coupled mode equations we can easily show that $a_j^*(-y)$ is also a solution by simply inserting it into (2.33) which yields

$$\sigma_{ij}(y) (a_j^*(-y))' = c_{ij}(y) a_j^*(-y) \quad (2.42)$$

where we again made use of Einstein's summation convention. After using that

$$\sigma_{ij}(-y) = \sigma_{ij}^*(y) \text{ and } c_{ij}(-y) = -c_{ij}^*(y) \quad (2.43)$$

which can be derived from the left-right symmetry of our problem, as already stated before, we arrive at

$$-\sigma_{ij}^*(-y) a_j'^*(-y) = -c_{ij}^*(-y) a_j^*(-y). \quad (2.44)$$

Finally substituting $y \rightarrow -y$ and conjugating the whole equation yields

$$\sigma_{ij}(y) a_j'(y) = c_{ij}(y) a_j(y) \quad (2.45)$$

which is true since our premise was that $a_j(y)$ shall be a solution of the coupled mode equations.

In order not to break the left-right symmetry artificially we will in the following choose $y_{min} = -y_{max}$. Since both $a_j(y)$ and $a_j^*(-y)$ solve the coupled mode equations (2.33) they therefore also have to satisfy (2.36), i.e.

$$\begin{pmatrix} a_r(y_{max}) \\ a_w(y_{max}) \end{pmatrix} = T \begin{pmatrix} a_r(y_{min}) \\ a_w(y_{min}) \end{pmatrix} \quad \text{and} \quad \begin{pmatrix} a_r^*(-y_{max}) \\ a_w^*(-y_{max}) \end{pmatrix} = T \begin{pmatrix} a_r^*(-y_{min}) \\ a_w^*(-y_{min}) \end{pmatrix}. \quad (2.46)$$

Using that the propagation matrix T also has to be unitary, the last matrix equation in (2.46) can be rewritten as

$$\begin{pmatrix} a_r(y_{max}) \\ a_w(y_{max}) \end{pmatrix} = T^\top \begin{pmatrix} a_r(y_{min}) \\ a_w(y_{min}) \end{pmatrix}. \quad (2.47)$$

Because the equations in (2.46) and (2.47) must hold for every pair of incoming amplitudes we can conclude that T must be symmetric.

2.3 Sample Calculations for Optical Conveyor Belt

Lastly, we are going to show the results of some sample calculations that we performed to investigate if an optical conveyor belt as described, e.g. in [22], can work when the fiber is in the near vicinity of a bottle resonator. The purpose of such a conveyor belt is to be able to transport cold atoms along long distances,⁹ ideally without loss of coherence. To do this an ultra-thin waveguide, like the coupling fiber for our bottle resonator, is used into which laser light is injected. The evanescent electromagnetic field surrounding the fiber creates a periodic trap potential for the desired atoms. By shifting the phase of the incoming light the atoms inside the trap can simply be moved as the periodic potential is translated along the fiber.

However, moving the atoms along the fiber is not a purpose of its own but the actual aim rather is to bring the atoms close to some sort of device, for example the bottle resonator, with which they could interact. The problem that might now arise is that the electromagnetic field around the fiber may be altered by the presence of such a cavity and its property of being a trapping potential may be destroyed. This could happen because the laser light inside the waveguide may couple strongly enough into the resonator to create an evanescent field around it so powerful to realize such a scenario. Of course, this would mean that the atoms would fall out of the trap which would make the conveyor belt useless for bringing them near a bottle resonator. In order to prevent such a negative result in the experiment, we used the coupled mode theory as described in this chapter to investigate the this problem in detail.

⁹ i.e. a few millimeters

r_{wg}	β	$ T_{rw} $	τ_c
250 nm	$9.57 \mu\text{m}^{-1}$	0.0010	1100 ns
260 nm	$9.69 \mu\text{m}^{-1}$	0.0016	420 ns
270 nm	$9.80 \mu\text{m}^{-1}$	0.0024	190 ns
280 nm	$9.90 \mu\text{m}^{-1}$	0.0034	95 ns
300 nm	$10.3 \mu\text{m}^{-1}$	0.0055	36 ns
330 nm	$10.6 \mu\text{m}^{-1}$	0.0084	16 ns
400 nm	$10.7 \mu\text{m}^{-1}$	0.0105	10 ns

Table 2.1: The table shows the results which were calculated for the mentioned parameters in the text and different fiber radii according to the coupled mode theory as described in this chapter.

For the corresponding calculations, the dimensions of the resonator were chosen to be $18 \mu\text{m}$ for its radius r_0 , $0.012 \mu\text{m}^{-1}$ for its curvature Δk and 330 nm for its surface-to-surface distance d_{gap} to the waveguide. The fiber was positioned to pass the resonator at its waist so that it only couples significantly to modes with an axial wave number $q = 0$. Furthermore, the vacuum wavelength of the injected light was set to be 780 nm which, in conjunction with the aforementioned parameters, means that it most strongly couples to resonator modes with an azimuthal wave number of $m = 202$. Additionally, the polarization of the light was chosen such that it would only couple to TE-modes of the bottle resonator. As always, the waveguide mode in operation was set to be the fundamental mode HE_{11} .

The result of the calculations with the above parameters and for varying fiber radii r_{wg} are shown in Table 2.1 where τ_c denotes the coupling-induced decay time which we will later precisely define, cf. (3.4) and (3.20). As for now, one can think of τ_c as a measure for how strongly the resonator is disturbed by the waveguide. Additionally, the propagation constant β of the fiber mode was also included into the table, which is depended on r_{wg} .

It can be clearly seen from Table 2.1 that τ_c heavily increases for decreasing r_{wg} , making the resonator less "visible" for the light in the waveguide. This occurrence correlates with a deteriorated phase matching, which is defined to be achieved when

$$b \approx \frac{m}{r_0} = 11.2 \text{ nm}^{-1}. \quad (2.48)$$

Moreover, an in-depth analysis of how the computations arrived at this result further indicated that the phase mismatching for smaller radii is the main reason for the higher decay times. This effect can be thought of in the following way: light may couple into the resonator along the coupling region but interferes destructively inside of the cavity and is thus prevented from actually transferring energy. Therefore, the main conclusion from our computations is that by deliberately choosing a small fiber radius and thus having a poor phase matching, the resonator can be

made (almost) invisible for the laser light inside the waveguide. Furthermore, it shall be noted that making the radius of the waveguide small is even advantageous for the conveyor belt since it increases the strength of the evanescent electromagnetic field around the fiber and therefore the trapping potential. This result thus provides strong evidence for the experimental feasibility of the envisioned atom conveyor belt. An experimental implementation in the group of Arno Rauschenbeutel is presently in progress.

3 Scattering Matrix Models

In this chapter we will develop models which aim to properly describe the transmission and reflection spectra of our bottle resonator-waveguide system. Scattering matrices will be used to model the interaction between the different modes under consideration.

The coupling region of the fiber and the resonator will be modelled by means of a propagation matrix as introduced in the previous chapter. Consequently all earlier mentioned assumptions necessary for the coupled mode theory to be valid also apply to the current chapter. Most importantly, we will always assume that the fiber is sufficiently far apart from the bottle resonator such that the coupling is adiabatic, i.e. no backscattering or dissipation shall occur at the coupling region.

First, we will start with a simple model that only includes dissipation in the resonator, but no scattering, to introduce some basic ideas for this simpler setting. To be specific, the scattering between the degenerate clockwise and counterclockwise propagating resonator modes will be neglected for this case. In a next step this model will be extended to also account for scattering between the two counterpropagating resonator modes. For both cases explicit formulas for the amplitudes of all the modes involved will be given. Expressions for transmission and reflection can then also be easily derived. Exemplary spectra for reasonable parameters will be shown to visualize these formulas. Furthermore, conditions which ensure that the energy flux in the bottle resonator is conserved, or at least can only be dissipated, will be deduced. Throughout the work we will also obtain various relations between the parameters of the model and physical quantities which can be gained from experimental measurements.

A simpler but similar approach to describe the transmission of a fiber evanescently coupled to a resonator (namely a microsphere) has been used in reference [23].

3.1 Two-Mode Model

As already mentioned we will first only consider dissipation in the bottle resonator for the following simple two-mode model. Any backscattering, be it at the coupling region or inside the resonator, will be neglected. An illustration of the model described in this section is depicted in Fig. 3.1.

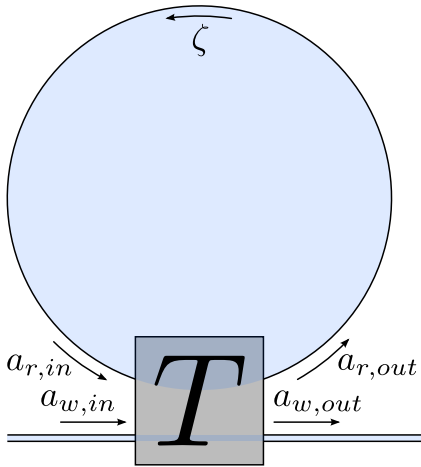


Figure 3.1: Block diagram to illustrate the model described in this section. The propagation matrix T relates the amplitudes before the coupling region to the ones after it and the round-trip factor ζ accounts for the dissipation in the resonator. Furthermore, the factor ζ also includes the phase mismatch between the amplitudes $a_{r,in}$ and $a_{r,out}$ when the driving frequency of the injected light is off-resonance in respect to the eigenfrequency of the resonator mode.

Let us assume that we have chosen a particular counterclockwise (CCW) resonator mode which we would like to excite. In order to do this, the incoming light in the waveguide must propagate from left to right (LtR), have a frequency (almost) equal to the eigenfrequency of the resonator mode¹⁰ and have the correct polarization (cf. 2.2.1). Since no backscattering shall be present at the coupling region or inside the bottle resonator we don't have to consider the waveguide mode of the same frequency that travels from right to left (RtL) nor the clockwise (CW) propagating version of the above CCW-mode. All other existing modes won't play a role due to the coupling conditions previously explained under 2.2.1. Thus, for the current case, we can limit ourselves to only dealing with the CCW- and LtR-mode (we could have chosen the CW- and RtL-mode as well), hence the name "two-mode model" was chosen. In this context we obviously have to assume that the light is injected into the resonator from the left side. The directions "left to right", "right to left", "clockwise" and "counterclockwise" are to be understood in reference to Fig. 3.1.

3.1.1 Basic Equations of the Model

With the above mentioned considerations in mind we can now start with establishing all necessary equations for our simple model. The amplitudes of the fiber mode before (after) the coupling region shall be denoted by $a_{w,in}$ ($a_{w,out}$) and the amplitude of the resonator mode before (after) the coupling region shall be denoted by $a_{r,in}$ ($a_{r,out}$).

¹⁰ To be precise, we should rather speak of an eigenfrequency for the whole resonator-waveguide system since the presence of the waveguide can shift the resonance.

Normalization

Due to the linearity of the problem any set of amplitudes that is a solution can be scaled with an arbitrary factor and still remains a solution. Therefore, without loss of generality, we shall assume that the amplitude of the injected light is equal to one, i.e.

$$a_{w,in} = 1. \quad (3.1)$$

Propagation Matrix

To describe the coupling between the CCW- and LtR-mode we can remind ourselves of equation (2.36) from the previous chapter, which is exactly what we are looking for. Therefore, just repeating (2.36), we get

$$\vec{a}_{out} = T \vec{a}_{in} \quad \text{with} \quad (3.2)$$

$$\vec{a}_{in} = \begin{pmatrix} a_{r,in} \\ a_{w,in} \end{pmatrix} \quad \text{and} \quad \vec{a}_{out} = \begin{pmatrix} a_{r,out} \\ a_{w,out} \end{pmatrix}$$

where T denotes the propagation matrix. The coupled mode theory from the chapter before can be used to calculate T for concrete parameters.

Nonetheless, without limiting ourselves to specific values, a general propagation matrix that accounts for time reversal symmetry, left-right symmetry and energy flux conservation, i.e. fulfills (cf. 2.2.4)

$$T^T = T \quad \text{and} \quad T^\dagger T = I \quad \text{with} \quad I := \begin{pmatrix} 1 & 0 \\ 0 & 1 \end{pmatrix} \quad (3.3)$$

can be represented by

$$T = \begin{pmatrix} a e^{i\alpha} & i b e^{i\beta} \\ i b e^{i\beta} & a e^{i\delta} \end{pmatrix} \quad \text{with} \quad a^2 + b^2 = 1 \quad \text{and} \quad \beta = \frac{\alpha + \delta}{2}. \quad (3.4)$$

The constants a and b are positive real numbers where b is a measure for the coupling strength. In accordance with calculations from the coupled mode theory we will assume the parameter b to be small, i.e. $b \ll 1$, although the properties of the propagation matrix as in (3.3) permit b to be in the range of $[0, 1]$. Consequently, a will almost be equal to one. The phases α , β and δ are also real numbers and can be restricted¹¹ to lie within the interval $[-\pi, \pi]$.

¹¹ obviously without loss of generality

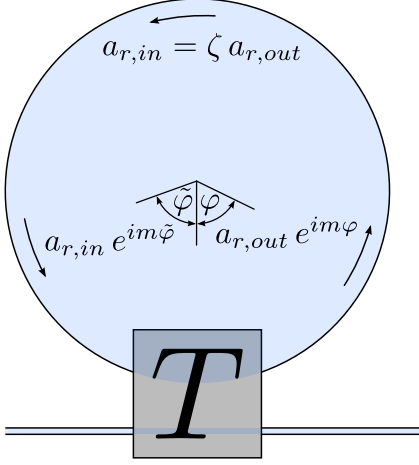


Figure 3.2: Depiction to visualize the derivation of the round-trip factor ζ . The amplitude of the CCW-mode before ($a_{r,in}$) and after ($a_{r,out}$) the coupling region have to be in accordance with each other, such that they give rise to the same electromagnetic field. When the angles φ and $\tilde{\varphi}$ refer to the same position they have to (in absolute values) add up to a full circle, i.e. $\varphi - \tilde{\varphi} = 2\pi$.

Round-Trip Factor

Now the only open question left is what happens when the light inside the bottle resonator revolves around and re-enters the coupling region. It is important to note that all our amplitudes are only meaningful when the form of the modes they relate to is exactly specified. In the following we will assume a time dependence of $e^{-i\omega t}$ for all the modes and thus the angular dependence of the CCW-mode must be of the form $e^{im\varphi}$.¹² Other dependencies and the vector form of the modes can be found under 2.1.2. With that the electromagnetic field outside the coupling region can be given in terms of either the amplitude $a_{r,in}$ or $a_{r,out}$, which has to give the same result. Therefore simply equating the electromagnetic fields as given by these two amplitudes multiplied with the CCW-mode yields

$$a_{r,in} e^{im\tilde{\varphi}} = a_{r,out} e^{im\varphi} \quad (3.5)$$

$$\text{with } \varphi - \tilde{\varphi} = 2\pi$$

as illustrated in Fig. 3.2. In the above equation we have omitted all dependencies of the modes, except of φ and $\tilde{\varphi}$, and that they are actually vectors because this is of no relevance here. After eliminating φ and $\tilde{\varphi}$ in (3.5) by multiplying with $e^{-im\tilde{\varphi}}$ we arrive at

$$a_{r,in} = a_{r,out} e^{2\pi i m}. \quad (3.6)$$

Since we would like to know the behaviour (e.g. the transmission) of our waveguide-resonator system in dependence of the frequency f of the injected light, f will in general not be equal to the eigenfrequency f_0 of the resonator mode. Consequently, the azimuthal wave number m will not be an integer. However, since only a detuning $\Delta f = f - f_0$ within the interval $[-\frac{\text{FSR}m}{2}, \frac{\text{FSR}m}{2}]$ makes sense,¹³ m is very well

¹² We will use the variable φ ($\tilde{\varphi}$) when the CCW-mode is multiplied with $a_{r,out}$ ($a_{r,in}$).

¹³ Otherwise we should reconsider which resonator mode we would like to excite (see the following paragraph for the definition of FSRm).

approximated by its Taylor expansion around f_0

$$m(f) = m(f_0) + \Delta f \frac{\partial m}{\partial f} = m_0 + \Delta f / \text{FSR}_m \quad \text{with} \quad (3.7)$$

$$m(f_0) = m_0 \in \mathbb{N} \quad \text{and} \quad \frac{\partial m}{\partial f} = 1 / \text{FSR}_m$$

where m_0 is an integer and denotes the azimuthal wave number of the CCW-mode with resonance frequency f_0 . The (azimuthal) free spectral range FSR_m denotes the difference of the eigenfrequencies of two resonator modes whose azimuthal wave number differ by one.

Finally, using the relations from (3.7) in equation (3.6) we deduce that

$$a_{r,in} = a_{r,out} e^{2\pi i m} = a_{r,out} e^{2\pi i m_0} e^{2\pi i \frac{\Delta f}{\text{FSR}_m}} = a_{r,out} e^{i \frac{2\pi \Delta f}{\text{FSR}_m}} \quad (3.8)$$

where we used that $e^{2\pi i m_0} = 1$. Additionally, allowing the resonator to exhibit dissipation yields

$$a_{r,in} = \zeta a_{r,out} \quad \text{with} \quad \zeta = (1 - \varepsilon) e^{i \frac{2\pi \Delta f}{\text{FSR}_m}}. \quad (3.9)$$

where the factor $(1 - \varepsilon)$ has been introduced heuristically. We will call ζ the round-trip factor and will refer to $e^{i \frac{2\pi \Delta f}{\text{FSR}_m}}$ as the round-trip phase shift. Since the bottle resonator has a high (intrinsic) quality factor Q_0 we will only consider small dissipations, i.e. $\varepsilon \ll 1$. Note that

$$\varepsilon \geq 0 \quad (3.10)$$

has to hold because the energy in our system can only be dissipated and not amplified.

3.1.2 Decay Time

Quality Factor and Dissipation

Moreover, within the framework of our model, we can directly relate the dissipation ε and the quality factor Q_0 with each other. To do this one has to investigate how these two quantities determine the (intrinsic) decay time τ_0 of light inside the bottle resonator when no fiber were present. On the one hand, the quality factor is defined as

$$Q_0 = 2\pi f \tau_0 \quad (3.11)$$

where f denotes the frequency of the confined light. Thus the decay time can simply be written as

$$\tau_0 = \frac{Q_0}{2\pi f}. \quad (3.12)$$

On the other hand, the amplitude of the CCW-mode after one revolution is decreased by the factor $(1 - \varepsilon)$. Furthermore, we also know that, for a given decay time τ_0 , the amplitude after a time t is reduced by the factor e^{-t/τ_0} . Now we only need an expression for the period T ,¹⁴ i.e. the time it takes the light for one rotation, which is approximately given by

$$T \approx \frac{2\pi r_0}{c/n_{sil}} \quad (3.13)$$

with radius of the bottle resonator r_0 . The term c/n_{sil} denotes the speed of light in silica and thus (3.13) just calculates how long it takes the light to cover the distance of the resonator's circumference. Note that, since the bottle resonator mode is partially located outside the glass, the real value of T will be a little bit smaller than calculated from above approximation.

Obviously, the two obtained factors should coincide and thus equating them yields

$$e^{-T/\tau_0} = (1 - \varepsilon). \quad (3.14)$$

Since the decay time τ_0 is much larger, especially for high quality factors, than the period T we can Taylor expand the exponential function to the first order and arrive at the formula

$$T/\tau_0 = \varepsilon \quad (3.15)$$

for the dissipation. Finally, using equations (3.13) and (3.12) results in

$$\varepsilon \approx \frac{2\pi r_0 / \frac{c}{n_{sil}}}{Q_0 / 2\pi f}. \quad (3.16)$$

Inserting typical values for f , r_0 and Q_0 shows that the dissipation ε is indeed small as expected.

Coupling-Induced Decay Time

For the sake of completeness we will also give an expression for the coupling-induced decay time τ_c . As before, the amplitude of the CCW-mode is decreased by $(1 - \varepsilon)$ after one revolution. However, we also have to take the coupling region into account. Looking at equations (3.2) and (3.4) and since no light shall be injected into the fiber, i.e. $a_{w,in} = 0$, it is clear that the CCW-mode is additionally decreased by a factor $a = \sqrt{1 - b^2} \approx 1 - \frac{b^2}{2}$. Therefore, in analogy to before, we obtain

$$e^{-T/\tau} = \sqrt{1 - b^2} (1 - \varepsilon), \quad (3.17)$$

¹⁴ not to be confused with the propagation matrix

where τ denotes the overall decay time of the whole system. Finally, after Taylor expanding the exponential function and neglecting all terms of higher order we get

$$T/\tau = \varepsilon + \frac{b^2}{2} \quad (3.18)$$

or equivalently

$$\tau = \frac{T}{\varepsilon + \frac{b^2}{2}}. \quad (3.19)$$

After defining the coupling-induced decay time as

$$\tau_c := \frac{T}{b^2/2}, \quad (3.20)$$

which is a measure for how strongly the resonator is disturbed by the fiber, equation (3.19) can be rewritten as

$$\frac{1}{\tau} = \frac{1}{\tau_0} + \frac{1}{\tau_c}. \quad (3.21)$$

Above equations show that the dissipation ε in (3.15) should be replaced by an "effective dissipation" $\varepsilon + \frac{b^2}{2}$ to arrive at the same result.

3.1.3 Solution of the Equations

With all necessary equations, i.e. (3.1), (3.2) and (3.9), now being established, we would like to find their solution. Due to the linearity of the problem this is an easy task and the amplitudes in dependence of the detuning Δf are given by

$$a_{r,out} = \frac{i b e^{i\frac{\alpha+\delta}{2}}}{1 - \sqrt{1-b^2} (1-\varepsilon) e^{i(\frac{2\pi\Delta f}{\text{FSR}_m} + \alpha)}} \quad (3.22)$$

$$a_{w,out} = e^{i\delta} \frac{\sqrt{1-b^2} - (1-\varepsilon) e^{i(\frac{2\pi\Delta f}{\text{FSR}_m} + \alpha)}}{1 - \sqrt{1-b^2} (1-\varepsilon) e^{i(\frac{2\pi\Delta f}{\text{FSR}_m} + \alpha)}}.$$

The formula for $a_{r,in}$ has been omitted since it is redundant, cf. (3.9). As can readily be seen in (3.22), the parameters α and δ only alter the phase of the amplitudes and α additionally shifts the position of the resonance. Moreover, only small values are of interest for the expression $(\frac{2\pi\Delta f}{\text{FSR}_m} + \alpha)$, which measures the detuning with respect to the shifted resonance, due to the narrow resonance width FWHM¹⁵ of a resonator with a high quality factor Q_0 .

Because the dissipation ε , the coupling strength b and the expression $(\frac{2\pi\Delta f}{\text{FSR}_m} + \alpha)$ are small we can make a Taylor expansion in these three terms in both the

¹⁵ i.e. full width at half maximum

numerator and denominator in the above formulas and can neglect all terms except those of lowest order. After doing that we obtain the following expressions for the amplitudes

$$a_{r,out} \approx -\frac{ib e^{i\frac{\alpha+\delta}{2}}}{i\left(\frac{2\pi\Delta f}{\text{FSRm}} + \alpha\right) - \left(\varepsilon + \frac{b^2}{2}\right)} \quad (3.23)$$

$$a_{w,out} \approx e^{i\delta} \frac{i\left(\frac{2\pi\Delta f}{\text{FSRm}} + \alpha\right) - \left(\varepsilon - \frac{b^2}{2}\right)}{i\left(\frac{2\pi\Delta f}{\text{FSRm}} + \alpha\right) - \left(\varepsilon + \frac{b^2}{2}\right)}$$

which are very good approximations for (3.22) under the mentioned assumptions.

Formulas for the squared absolute value of the amplitudes, which correspond to the intensity of the light, can easily be derived from (3.23) and are given by

$$|a_{r,out}|^2 \approx \frac{b^2}{\left(\frac{2\pi\Delta f}{\text{FSRm}} + \alpha\right)^2 + \left(\varepsilon + \frac{b^2}{2}\right)^2} \quad (3.24)$$

$$|a_{w,out}|^2 \approx 1 - \frac{2b^2\varepsilon}{\left(\frac{2\pi\Delta f}{\text{FSRm}} + \alpha\right)^2 + \left(\varepsilon + \frac{b^2}{2}\right)^2}$$

where $|a_{w,out}|^2$ already defines the transmission of the waveguide since $a_{w,in}$ was defined to equal one. As can be seen from above formulas the intensity of the light is given by a Lorentzian function as could have been expected.

Moreover, from (3.24) we can also derive when critical coupling is realized, i.e. when the resonance dip goes down to zero. It can easily be seen that the formula for the transmission has its minimum at $\Delta f = -\frac{\alpha}{2\pi} \text{FSRm}$ and reaches zero when

$$\varepsilon = \frac{b^2}{2}. \quad (3.25)$$

Note that b can still be small at critical coupling given that ε is also small. At smaller coupling strengths the resonator amplitude just becomes larger such that the coupled out light which interferes destructively with the one in the waveguide still annihilates it completely.

Furthermore, we can also deduce an expression for the resonance width FWHM from (3.24) which reads

$$\text{FWHM} = \frac{1}{\pi} \left(\varepsilon + \frac{b^2}{2} \right) \text{FSRm} \quad (3.26)$$

as can be checked by calculating $|a_{r,out}|^2$ for $\Delta f = -\frac{\alpha}{2\pi} \text{FSRm}$ and $\Delta f = -\frac{\alpha}{2\pi} \text{FSRm} + \frac{\text{FWHM}}{2}$ and comparing the results.

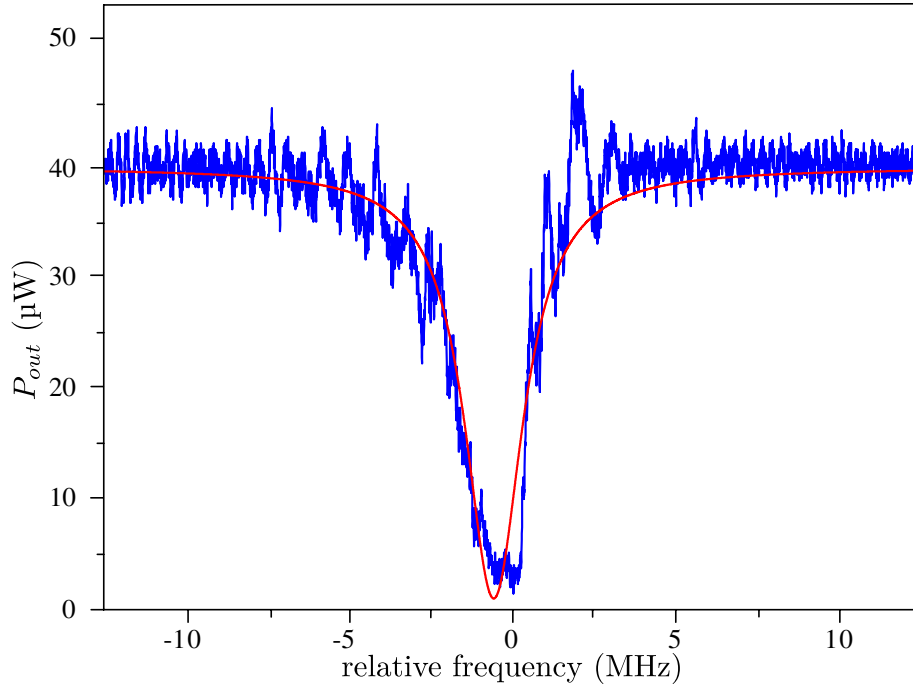


Figure 3.3: Experimentally measured transmission spectrum at critical coupling taken from reference [1]. The quantity P_{out} denotes the power of the transmitted light and the red line represents a Lorentzian fit of the data obtained from the experiment.

3.1.4 Exemplary Spectra

In the following, transmission spectra will be shown for some exemplary values of FSR_m, b and ε . Since α and δ can't change the shape of the spectrum we will set them equal zero, cf. (3.22).

To also get a feeling for the order of magnitude of our model parameters, and to verify that they are indeed small, we will try to reproduce the experimentally measured transmission spectrum shown in Fig. 2(b) of [1], reproduced here in Fig. 3.3.

From the parameters given in the reference we know that

$$\text{FSR}_m = 1.74 \text{ THz} \quad (3.27)$$

and that

$$\text{FWHM} = 2.1 \text{ MHz} \quad (3.28)$$

at critical coupling.

Using (3.25) and (3.26) we can derive an expression for the dissipation

$$\varepsilon = \frac{\pi \text{FWHM}}{2 \text{FSR}_m} \quad (3.29)$$

when the fiber is critically coupled to the resonator. Inserting the above mentioned values into (3.29) yields

$$\varepsilon \approx 2 \times 10^{-6}. \quad (3.30)$$

Moreover, after solving equation (3.25) for b we obtain

$$b = \sqrt{2\varepsilon} \quad (3.31)$$

and calculating the numerical value results in

$$b \approx 0.002 \quad (3.32)$$

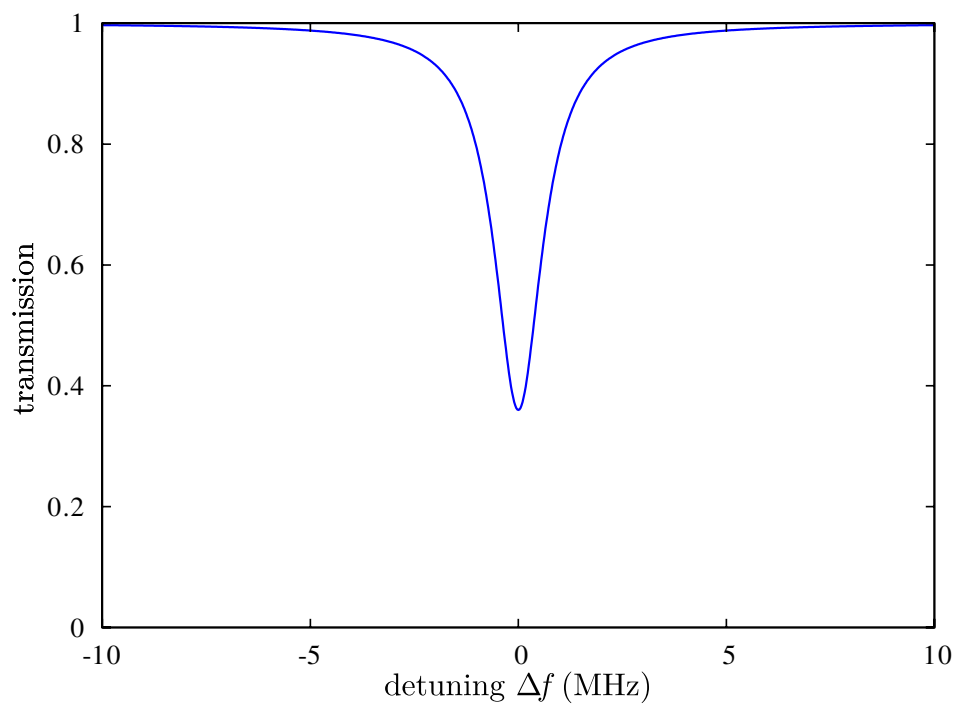
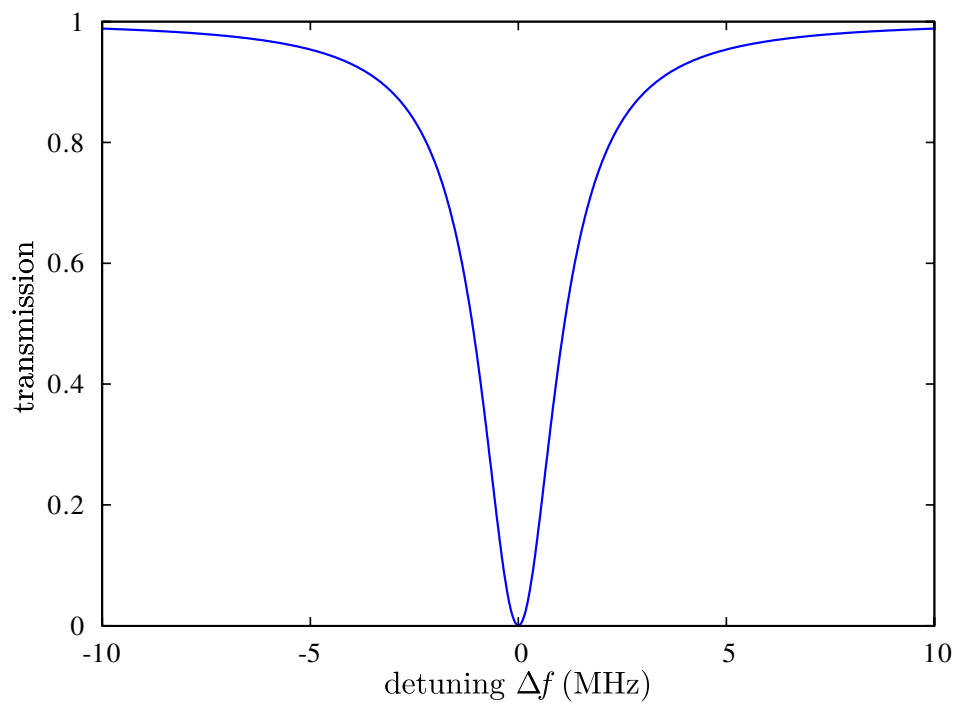
which is the coupling strength at critical coupling for above computed dissipation.

The transmission spectrum as determined by (3.22) or (3.23) with the parameters presented above [i.e. (3.27), (3.30) and (3.32)] is shown in Fig. 3.5. Looking at the diagram we observe that the transmission reaches zero as it should be for critical coupling. Additionally, an undercoupled (overcoupled) spectrum is shown in Fig. 3.4 (Fig. 3.6) for which only the coupling strength b has been changed, namely to $b = 0.001$ ($b = 0.003$). In the experiments the strength of the coupling is altered via reducing or increasing the distance between the waveguide and the bottle resonator.

Finally, we will investigate how well the approximation for $a_{w,out}$ in (3.22) agrees with the actual solution in (3.22). To do this the absolute value of the error Δ , i.e. the difference between the two expressions

$$\Delta = \left| \left(\frac{\sqrt{1-b^2} - (1-\varepsilon) e^{i(\frac{2\pi\Delta f}{\text{FSR}_m} + \alpha)}}{1 - \sqrt{1-b^2} (1-\varepsilon) e^{i(\frac{2\pi\Delta f}{\text{FSR}_m} + \alpha)}} \right) - \left(\frac{i(\frac{2\pi\Delta f}{\text{FSR}_m} + \alpha) + (\frac{b^2}{2} - \varepsilon)}{i(\frac{2\pi\Delta f}{\text{FSR}_m} + \alpha) - (\frac{b^2}{2} + \varepsilon)} \right) \right|, \quad (3.33)$$

is depicted in Fig. 3.7 and clearly shows that the error is negligible. A similar figure can also be made for $a_{r,out}$.

Figure 3.4: Transmission spectrum for $b = 0.001$ Figure 3.5: Transmission spectrum for $b = 0.002$

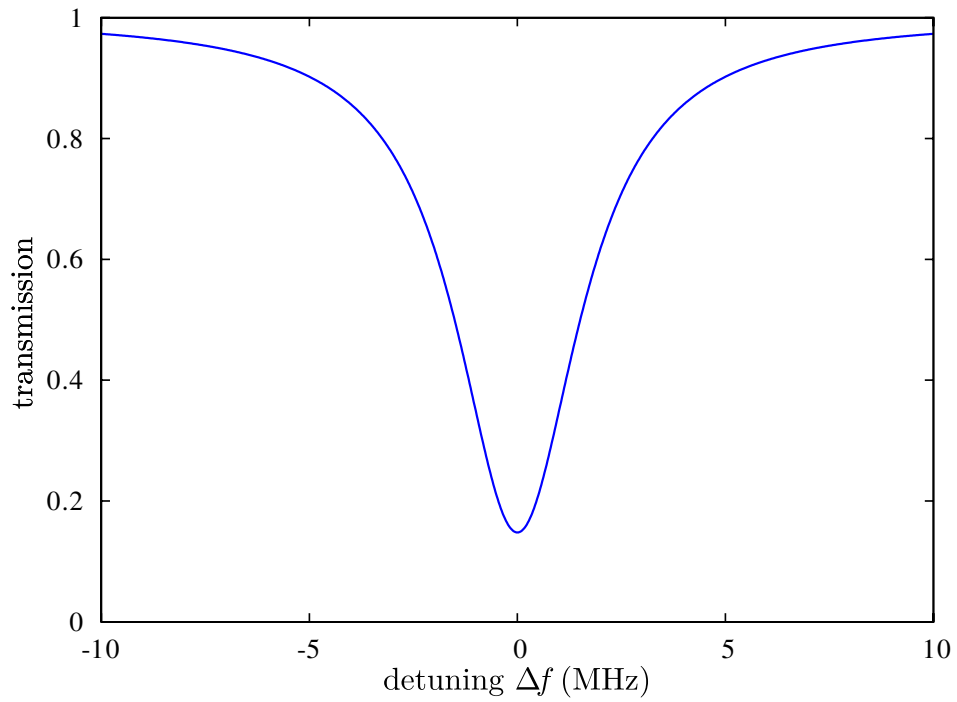


Figure 3.6: Transmission spectrum for $b = 0.003$

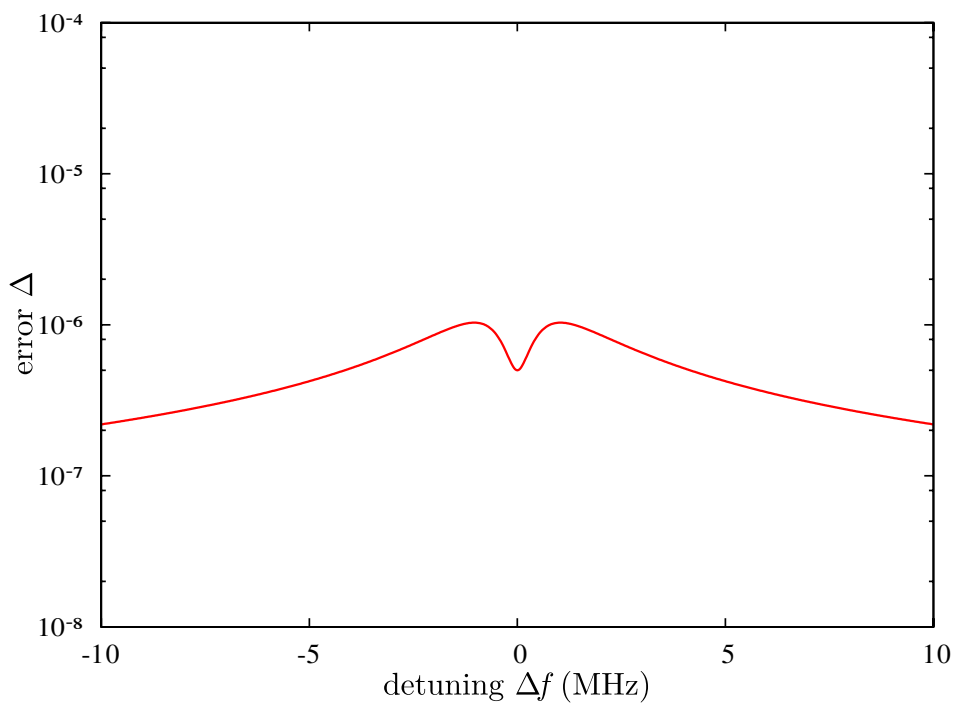


Figure 3.7: Absolute value of the error between the approximation for $a_{w,out}$ and its actual solution.

3.2 Four-Mode Model

In the following we will extend the previous two-mode model to also account for scattering inside the bottle resonator. Any dissipative or scattering processes that might occur within the resonator will be described by means of a scattering matrix. Again, no backscattering or dissipation shall occur at the coupling region. An illustration of the model we will develop in this section is depicted in Fig. 3.8.

Due to the scattering processes inside the bottle resonator permitted in the current model the CCW-mode now not only couples to the according LtR-mode but also to the CW-mode, i.e. the degenerate clockwise propagating version of the CCW-mode. Besides the LtR-mode, we also have to consider its counterpart, the RtL-mode, to which the CW-mode can couple into at the coupling region. As was already argued in the previous section, all other existing modes won't play a role due to the considerations mentioned under 2.2.1. Since a total of four modes need to be included into the model the name "four-mode model" was chosen.

Unlike before, we are so far free to choose if the light is injected from the right or the left side, but will investigate both cases. All above mentioned directions are to be understood in reference to Fig. 3.8.

3.2.1 Basic Equations of the Model

Establishing all necessary equations for the current four-mode model will be our next task. The amplitude of the LtR-mode before (after) the coupling region shall be denoted by $a_{w+,in}$ ($a_{w+,out}$) and the amplitudes of the RtL-mode before (after) the coupling region shall be denoted by $a_{w-,in}$ ($a_{w-,out}$). Similarly, the amplitude of the CCW-mode before (after) the coupling region shall be denoted by $a_{r+,in}$ ($a_{r+,out}$) and the amplitudes of the CW-mode before (after) the coupling region shall be denoted by $a_{r-,in}$ ($a_{r-,out}$). Furthermore, the amplitude of the CCW-mode before (after) all scattering and dissipative processes inside the resonator shall be denoted by $b_{r+,in}$ ($b_{r+,out}$) and the amplitude of the CW-mode before (after) all scattering and dissipative processes inside the resonator shall be denoted by $b_{r-,in}$ ($b_{r-,out}$). The reader may want to consult Fig. 3.8 for better understanding.

Normalization

As was already mentioned, the light in the fiber may be injected from the left, the right or even from both sides. However, we can restrict ourselves to the cases where the light comes solely from the left side

$$a_{w+,in} = 1 \quad \text{and} \quad a_{w-,in} = 0 \quad (3.34)$$

or solely from the right side

$$a_{w+,in} = 0 \quad \text{and} \quad a_{w-,in} = 1 \quad (3.35)$$

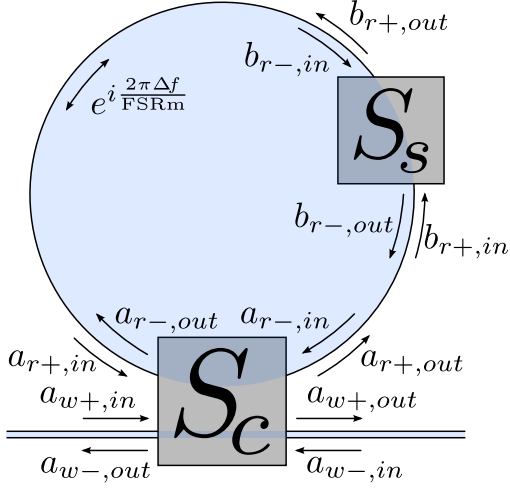


Figure 3.8: Block diagram to illustrate the model described in this section. The coupling matrix S_c relates the incoming scattering amplitudes (i.e. those with an "in" in the subscript) to the outgoing ones (i.e. those with an "out" in the subscript). Furthermore, any scattering or dissipation processes that might occur inside the resonator shall be subsumed into the scattering matrix S_s . Again, we have to account for a phase mismatch of $e^{i \frac{2\pi \Delta f}{\text{FSR}_m}}$ between the amplitudes after one revolution when the driving frequency of the injected light is off-resonance.

without loss of generality. The case where the light is injected from both sides can simply be reformulated as a superposition of the aforementioned cases due to the linearity of the problem. The same reason allowed us to have the incoming amplitudes in (3.35) and (3.34) already normalized to equal one.

Coupling Matrix

Again, the coupling between the CCW- and LtR-mode will be described via equation (2.36), i.e.

$$\vec{a}_{+,out} = T \vec{a}_{+,in} \quad \text{with} \quad (3.36)$$

$$\vec{a}_{+,in} = \begin{pmatrix} a_{r+,in} \\ a_{w+,in} \end{pmatrix} \quad \text{and} \quad \vec{a}_{+,out} = \begin{pmatrix} a_{r+,out} \\ a_{w+,out} \end{pmatrix},$$

where T , as previously, denotes the propagation matrix. In a similar manner we can also describe the coupling between the CW- and RtL-mode, namely

$$\vec{a}_{-,out} = T \vec{a}_{-,in} \quad \text{with} \quad (3.37)$$

$$\vec{a}_{-,in} = \begin{pmatrix} a_{r-,in} \\ a_{w-,in} \end{pmatrix} \quad \text{and} \quad \vec{a}_{-,out} = \begin{pmatrix} a_{r-,out} \\ a_{w-,out} \end{pmatrix},$$

where the propagation matrix T must be the same as in (3.36) due to the left-right symmetry of the coupling region. Finally, rewriting equations (3.36) and (3.37) in a more compact way results in

$$\vec{a}_{out} = S_c \vec{a}_{in} \quad \text{with} \quad S_c = \begin{pmatrix} 0_2 & T \\ T & 0_2 \end{pmatrix}, \quad (3.38)$$

$$\vec{a}_{in} = \begin{pmatrix} a_{r+,in} \\ a_{w+,in} \\ a_{r-,in} \\ a_{w-,in} \end{pmatrix} \quad \text{and} \quad \vec{a}_{out} = \begin{pmatrix} a_{r-,out} \\ a_{w-,out} \\ a_{r+,out} \\ a_{w+,out} \end{pmatrix}$$

where the coupling matrix S_c actually is a 4×4 scattering matrix. The 2×2 zero matrices denoted by 0_2 in the definition of S_c represent the assumption that no backscattering shall occur at the coupling region.

Like in the two-mode model before we don't want to limit ourselves to a specific propagation matrix, and thus coupling matrix, and will therefore use the same general expression

$$T = \begin{pmatrix} a e^{i\alpha} & i b e^{i\beta} \\ i b e^{i\beta} & a e^{i\delta} \end{pmatrix} \quad \text{with} \quad a^2 + b^2 = 1 \quad \text{and} \quad \beta = \frac{\alpha + \delta}{2} \quad (3.39)$$

as in (3.4) for the propagation matrix.

Note that the properties of the propagation matrix, cf. (3.3), already account for time reversal symmetry

$$S_c^T = S_c \quad (3.40)$$

and energy flux conservation

$$S_c^\dagger S_c = I \quad (3.41)$$

of the coupling matrix. Due to the left-right symmetry S_c can be written as

$$S_c = \begin{pmatrix} A & B \\ B & A \end{pmatrix} \quad \text{with} \quad A, B \in \mathbb{M}(2, 2), \quad (3.42)$$

and since no backscattering shall occur at the coupling region we can further write

$$A = 0_2. \quad (3.43)$$

Note that the equations (3.42) and (3.43) already follow from the definition of the coupling matrix in (3.38). In fact, the properties of the propagation matrix, cf. (3.3), and those of the coupling matrix, cf. (3.40)-(3.43), are actually equivalent and imply each other.

A more general form of the coupling matrix which does not assume that no backscattering shall occur at the coupling region was derived in the course of this work and can be found in chapter 6. However, we are not going to investigate what implications such a general coupling matrix would or would not yield in the following.

Scattering Matrix

Unlike before, we will not only account for any dissipation process but also for any scattering process that might take place within the bottle resonator and which gives

rise to an interaction between the CW- and CCW-mode. The relation between the amplitudes of the resonator modes before any scattering or dissipation and the ones after it will be modelled by means of a scattering matrix. Hence we write

$$\vec{b}_{out} = S_s \vec{b}_{in} \quad (3.44)$$

$$\text{with } \vec{b}_{in} = \begin{pmatrix} b_{r+,in} \\ b_{r-,in} \end{pmatrix} \quad \text{and} \quad \vec{b}_{out} = \begin{pmatrix} b_{r-,out} \\ b_{r+,out} \end{pmatrix}$$

where the scattering matrix S_s shall subsume all the scattering processes but also any dissipation that might occur inside the resonator.

Due to time reversal symmetry, which originates from Maxwell's equations, the scattering matrix must fulfil

$$S_s^T = S_s. \quad (3.45)$$

Obviously, the following representation of the scattering matrix

$$S_s = e^{i\theta} \begin{pmatrix} i r_p & 1 - \varepsilon \\ 1 - \varepsilon & i r_m \end{pmatrix} \quad (3.46)$$

$$\text{with } \varepsilon, \theta \in \mathbb{R} \quad \text{and} \quad r_p, r_m \in \mathbb{C}$$

complies with (3.45), where the parameter θ can generally be assumed to lie within the interval $[-\pi, \pi]$. The parameter ε is a measure for the dissipation and r_p (r_m) correlates to the fraction of the CCW-mode (CW-mode) that is reflected back into the CW-mode (CCW-mode) after one revolution. From now on we may refer to ε as the dissipation and to r_p and r_m as reflections strengths whose values are all deemed to be small since we are only interested in bottle resonators with a high quality factor Q_0 . Moreover, it should be mentioned that the two-mode model is just a special case of the four-mode model when $r_p = 0$ and when the light is injected from the left side, i.e. equation (3.34) is used in contrast to (3.35).

Unitarity of the scattering matrix it would follow that $r_p = r_m^*$ which could still break the left-right symmetry. However, Note that, we won't require $S_s^\dagger S_s = I$ to hold, because the energy flux is generally not conserved since the light may e.g. scatter into free space modes and thus out of the resonator. Correspondingly, the amplitudes of the resonator modes in \vec{b}_{in} and \vec{b}_{out} have to satisfy

$$|b_{r+,out}|^2 + |b_{r-,out}|^2 \leq |b_{r+,in}|^2 + |b_{r-,in}|^2 \quad (3.47)$$

since their squared absolute value is proportional to the energy flux.¹⁶ Equivalently, (3.47) can be written as

$$\|S_s\| \leq 1 \quad (3.48)$$

¹⁶ The squared absolute values actually already equal the energy flux because we assumed in 2.2.4 that the modes are accordingly normalized.

where

$$\|S_s\| := \max\{\|A\vec{x}\| : \vec{x} \in \mathbb{R}^2 \text{ with } \|\vec{x}\| = 1\} \quad (3.49)$$

denotes the matrix norm of S_s . After a quite tedious derivation one can deduce that

$$\|S_s\|^2 = (1 - \varepsilon)^2 + \frac{|r_p|^2 + |r_m|^2}{2} + \sqrt{(1 - \varepsilon)^2 |r_p - r_m^*|^2 + \left(\frac{|r_p|^2 - |r_m|^2}{2}\right)^2}. \quad (3.50)$$

Since the parameters ε , r_p and r_m shall be small we can make a Taylor expansion and neglect all terms of higher order. Additionally, making use of the inequality (3.48) finally yields the condition

$$\varepsilon \gtrsim \frac{|r_p - r_m^*|}{2} = \frac{|r_p r_m - |r_p|^2|}{2|r_p|} = \frac{|r_p r_m - |r_m|^2|}{2|r_m|} \quad (3.51)$$

which the parameters have to obey so that energy may only be dissipated or conserved but not created.

Be aware that the scattering matrix in general (if $r_p \neq r_m$) breaks the left-right symmetry of the whole system and can thus give rise to different spectra when the light is injected from the left- or right-hand side. Even if we were to demand the scattering matrix to be unitary it would only follow that $r_p = r_m^*$ which could still break the left-right symmetry. However, this wouldn't give rise for any asymmetry at the spectra as can be seen from the formulas we will derive later on.

Round-Trip Phase Shift

At last, we have to explain how the amplitudes $a_{r+,in}$, $a_{r-,in}$, $a_{r+,out}$ and $a_{r-,out}$ are linked to the amplitudes $b_{r+,in}$, $b_{r-,in}$, $b_{r+,out}$ and $b_{r-,out}$. Since nothing should happen between the coupling region and the sector of the resonator where scattering or dissipation may occur we stipulate that the amplitudes shall satisfy

$$a_{r+,out} = b_{r+,in} \quad \text{and} \quad b_{r-,out} = a_{r-,in}. \quad (3.52)$$

Beware that, after a full revolution, we need to take care of a round-trip phase shift, as we previously derived under 3.1.1. Therefore the other amplitudes have to obey

$$a_{r+,in} = b_{r+,out} e^{i \frac{2\pi \Delta f}{\text{FSR}_m}} \quad \text{and} \quad b_{r-,in} = a_{r-,out} e^{i \frac{2\pi \Delta f}{\text{FSR}_m}} \quad (3.53)$$

which completes the set of equations for our four-mode model.

3.2.2 Solutions of the Equations

Exact Solutions

Since all necessary equations have now been established, we would like to find their solution. Due to the linearity of the problem this is (essentially) an easy task, although much more tedious than for the two-mode model because we have to solve for a lot more unknowns as before.

On the one hand, when the light is injected from the left side, i.e. our system of equations consists of (3.34), (3.38), (3.44), (3.52) and (3.53), the amplitudes in dependence of the detuning Δf are given by

$$\begin{aligned}
a_{r+,out}^l &= i \frac{b}{d} e^{i\frac{\alpha+\delta}{2}} \left(1 - \sqrt{1-b^2} (1-\varepsilon) e^{i\Delta p} \right) \\
b_{r+,out}^l &= i \frac{b}{d} e^{i\frac{\alpha+\delta}{2}} e^{i\theta} \left((1-\varepsilon) - \sqrt{1-b^2} \left((1-\varepsilon)^2 + r^2 \right) e^{i\Delta p} \right) \\
a_{r-,out}^l &= -r_p \frac{b}{d} \sqrt{1-b^2} e^{i\frac{\alpha+\delta}{2}} e^{i(\alpha+\theta)} \\
b_{r-,out}^l &= -r_p \frac{b}{d} e^{i\frac{\alpha+\delta}{2}} e^{i\theta} \\
a_{w+,out}^l &= \frac{e^{i\delta}}{d} \left(\sqrt{1-b^2} - 2 \left(1 - \frac{b^2}{2} \right) (1-\varepsilon) e^{i\Delta p} + \right. \\
&\quad \left. + \sqrt{1-b^2} \left((1-\varepsilon)^2 + r^2 \right) e^{2i\Delta p} \right) \\
a_{w-,out}^l &= -i r_p \frac{b^2}{d} e^{i\delta} e^{i(\alpha+\theta)}
\end{aligned} \tag{3.54}$$

where we used the abbreviations

$$\begin{aligned}
d &= \left(1 - \sqrt{1-b^2} (1-\varepsilon) e^{i\Delta p} \right)^2 + r^2 (1-b^2) e^{2i\Delta p} \\
&= 1 - 2\sqrt{1-b^2} (1-\varepsilon) e^{i\Delta p} + (1-b^2) \left((1-\varepsilon)^2 + r^2 \right) e^{2i\Delta p},
\end{aligned} \tag{3.55}$$

$$\Delta p = \frac{2\pi\Delta f}{\text{FSRm}} + \alpha + \theta \quad \text{and} \quad r = \sqrt{r_p r_m}.$$

In (3.54) we omitted the formulas for $b_{r+,in}^l$, $a_{r+,in}^l$, $b_{r-,in}^l$ and $a_{r-,in}^l$ since they would be redundant, c.f. (3.52) and (3.53).

On the other hand, when the light is injected from the right side, i.e. we replace (3.34) by (3.35) in our system of equations, the amplitudes are given by

$$\begin{aligned}
a_{r+,out}^r &= -r_m \frac{b}{d} \sqrt{1-b^2} e^{-i\frac{\alpha-\delta}{2}} e^{-i\theta} e^{2i\Delta p} \\
b_{r+,out}^r &= -r_m \frac{b}{d} e^{-i\frac{\alpha-\delta}{2}} e^{i\Delta p} \\
a_{r-,out}^r &= i \frac{b}{d} e^{i\frac{\alpha+\delta}{2}} \left(1 - \sqrt{1-b^2} (1-\varepsilon) e^{i\Delta p} \right) \\
b_{r-,out}^r &= i \frac{b}{d} e^{-i\frac{\alpha-\delta}{2}} e^{i\Delta p} \left((1-\varepsilon) - \sqrt{1-b^2} ((1-\varepsilon)^2 + r^2) e^{i\Delta p} \right) \\
a_{w+,out}^r &= -i r_m \frac{b^2}{d} e^{i\delta} e^{-i(\alpha+\theta)} e^{2i\Delta p} \\
a_{w-,out}^r &= \frac{e^{i\delta}}{d} \left(\sqrt{1-b^2} - 2 \left(1 - \frac{b^2}{2} \right) (1-\varepsilon) e^{i\Delta p} + \right. \\
&\quad \left. + \sqrt{1-b^2} ((1-\varepsilon)^2 + r^2) e^{2i\Delta p} \right)
\end{aligned} \tag{3.56}$$

where we again omitted the formulas for $b_{r+,in}^r$, $a_{r+,in}^r$, $b_{r-,in}^r$ and $a_{r-,in}^r$ due to redundancy and made use of the aforementioned abbreviations. The superscripts 'l' and 'r' were introduced to distinguish between the resulting amplitudes when the light is injected from the left or the right side, respectively.

As can readily be seen from (3.54), (3.55) and (3.56), the parameters α , δ and θ only alter the phase of the amplitudes and α and θ additionally shift the position of the resonance. Moreover, only small values are of interest for the expression $\left(\frac{2\pi\Delta f}{\text{FSR}_m} + \alpha + \theta \right)$, which measures the detuning in respect to the shifted resonance, due to the narrow resonance width of a resonator with a high quality factor.

Approximations

Because the dissipation ε , the reflection strengths r_p and r_m , the coupling strength b and the expression $\left(\frac{2\pi\Delta f}{\text{FSR}_m} + \alpha + \theta \right)$ are small we can make a Taylor expansion in these five terms in both the numerator and denominator in above formulas and neglect all terms except those of lowest order, like we did under 3.1.3. After doing that we get the following expressions for the amplitudes

$$\begin{aligned}
a_{r+,out}^l &= a_{r-,out}^r \approx e^{-i\theta} b_{r+,out}^l \approx e^{i\alpha} b_{r-,out}^r \approx -i \frac{b}{\tilde{d}} e^{i\frac{\alpha+\delta}{2}} \left(i \Delta p - \left(\varepsilon + \frac{b^2}{2} \right) \right) \\
a_{r-,out}^l &\approx e^{i\alpha} b_{r-,out}^l \approx -r_p \frac{b}{\tilde{d}} e^{i\frac{\alpha+\delta}{2}} e^{i(\alpha+\theta)} \\
a_{r+,out}^r &\approx e^{-i\theta} b_{r+,out}^r \approx -r_m \frac{b}{\tilde{d}} e^{-i\frac{\alpha-\delta}{2}} e^{-i\theta} \\
a_{w-,out}^l &\approx -i r_p \frac{b^2}{\tilde{d}} e^{i\delta} e^{i(\alpha+\theta)} \\
a_{w+,out}^r &\approx -i r_m \frac{b^2}{\tilde{d}} e^{i\delta} e^{-i(\alpha+\theta)} \\
a_{w+,out}^l &= a_{w-,out}^r \approx e^{i\delta} \left(1 + \frac{b^2}{\tilde{d}} \left(i \Delta p - \left(\varepsilon + \frac{b^2}{2} \right) \right) \right)
\end{aligned} \tag{3.57}$$

where we used the abbreviation

$$\tilde{d} = \left(i \Delta p - \left(\varepsilon + \frac{b^2}{2} \right) \right)^2 + r^2 \tag{3.58}$$

for the denominator. Under the mentioned assumptions, the above formulas are very good approximations for (3.54) and (3.56), as we will confirm later.

3.2.3 Transmissions and Reflections

To obtain formulas for the transmission and reflection of the light in the fiber we need to calculate the squared absolute value of the amplitudes of the waveguide modes. After quite a lengthy derivation in which we made use of the approximations in (3.57) we arrive at

$$\begin{aligned}
|a_{w+,out}^l|^2 = |a_{w-,out}^r|^2 &\approx 1 - b^2 \left(\frac{a_1}{(\Delta p - \mu)^2 + \Gamma_1^2} + \frac{a_2}{(\Delta p + \mu)^2 + \Gamma_2^2} \right) - \\
&\quad - b^4 \frac{|r_p r_m|}{((\Delta p + \mu)^2 + \Gamma_1^2)((\Delta p - \mu)^2 + \Gamma_2^2)} \\
\frac{|a_{w-,out}^l|^2}{|r_p|^2} = \frac{|a_{w+,out}^r|^2}{|r_m|^2} &= \frac{b^4}{|d|^2} \approx \frac{b^4}{((\Delta p + \mu)^2 + \Gamma_1^2)((\Delta p - \mu)^2 + \Gamma_2^2)}
\end{aligned} \tag{3.59}$$

where we used the abbreviations

$$\mu = \operatorname{Re}(r), \quad a_1 = \varepsilon - \operatorname{Im}(r), \quad a_2 = \varepsilon + \operatorname{Im}(r), \quad (3.60)$$

$$\Gamma_1 = \left(\varepsilon + \frac{b^2}{2} \right) - \operatorname{Im}(r) \quad \text{and} \quad \Gamma_2 = \left(\varepsilon + \frac{b^2}{2} \right) + \operatorname{Im}(r).$$

Consequently, the transmissions T^l and T^r and reflections R^l and R^r , which belong to the case where the light is injected from the right or left side respectively, are given by

$$T^l = |a_{w+,out}^l|^2 \quad \text{and} \quad R^l = |a_{w-,out}^l|^2 \quad (3.61)$$

and

$$T^r = |a_{w-,out}^r|^2 \quad \text{and} \quad R^r = |a_{w+,out}^r|^2 \quad (3.62)$$

since the incoming amplitudes were already normalized, cf. 3.2.1. According to (3.59) the transmissions T^l and T^r are equal and we will thus denote any transmission henceforth simply by T .¹⁷

Parameters from Experimentally Measured Spectra

A nice feature of the transmission spectrum and the two reflection spectra is that a sum of two Lorentzian functions can be constructed from them, i.e.

$$1 - T - \sqrt{R^l R^r} \approx b^2 \left(\frac{a_1}{(\Delta p - \mu)^2 + \Gamma_1^2} + \frac{a_2}{(\Delta p + \mu)^2 + \Gamma_2^2} \right), \quad (3.63)$$

as can be easily checked by looking at (3.59), (3.61) and (3.62). The relation in (3.63) can be used to obtain the parameters μ , a_1 , a_2 , Γ_1 and Γ_2 from experimentally measured spectra via simply fitting the expression $1 - T - \sqrt{R^l R^r}$ with a double-Lorentzian. During the fitting process one must be aware that the parameters cannot be chosen completely independently from each other but have to satisfy $a_2 - a_1 = \Gamma_2 - \Gamma_1$ as can clearly be seen from the equations in (3.60). Subsequently, the same equations can be used to obtain the formulas

$$b = \sqrt{(\Gamma_2 + \Gamma_1) - (a_2 + a_1)} \quad (3.64)$$

$$\varepsilon = \frac{a_2 + a_1}{2} \quad \text{and} \quad r = \mu + i \frac{a_2 - a_1}{2}$$

with which one can calculate the model-parameters b , ε and r from the fit-parameters μ , a_1 , a_2 , Γ_1 and Γ_2 .

Moreover, from the reflection spectra the ratio of the absolute values of the reflection strengths can be obtained through the equation

$$\sqrt{\frac{R^l}{R^r}} = \frac{|r_p|}{|r_m|} \quad (3.65)$$

¹⁷ not to be confused with the propagation matrix

which is derived from (3.61), (3.62) and (3.59). The relation (3.65) can be used to compute the absolute values of the reflection strengths $|r_p|$ and $|r_m|$ from R^l , R^r and r via

$$\begin{aligned} |r_p| &= \sqrt[4]{\frac{R^l}{R^r}} |r| \\ |r_m| &= \sqrt[4]{\frac{R^r}{R^l}} |r|. \end{aligned} \quad (3.66)$$

Consequently, one way to test the four-mode model described here would be to compute model-parameters for experimentally measured spectra according to (3.64) and to then check if they satisfy the inequality in (3.51). Obviously, another criterion for our model would be that the derived formulas, i.e. (3.57), (3.59), (3.61) and (3.62), should properly describe the amplitudes and spectra as observed in experiments.

3.2.4 Exemplary Spectra

In the following we will show transmission and reflection spectra for some exemplary values of FSRm, b , ε , r_p and r_m . Since α , δ and θ have no impact on the shape of the spectra, cf. the paragraph above 3.2.2, they can simply be set equal zero. Furthermore, we will also set $\text{Arg}(r_p) = \text{Arg}(r_m)$, due to the same reason. For the upcoming plots the same values as previously in 3.1.4 for the two-mode model will be used, namely

$$\begin{aligned} \text{FSRm} &= 1.74 \text{ THz} \\ b &= 0.002 \\ \varepsilon &= 2 \times 10^{-6} \end{aligned} \quad (3.67)$$

and for the reflection strengths we will choose

$$|r_p| = 3 \times 10^{-6} \quad \text{and} \quad |r_m| = 4 \times 10^{-6} \quad (3.68)$$

$$\text{with } \text{Arg}(r_p) = \text{Arg}(r_m) = 0.03 \pi.$$

Different absolute values were assigned to r_p and r_m in (3.68) to break the left-right symmetry of the system and to give thus rise to differing reflection spectra, as predicted by (3.59). Moreover, we have set $\text{Arg}(r_p) = \text{Arg}(r_m) \neq 0$ to introduce an asymmetry to the spectra according to (3.60). The transmission spectrum and reflection spectra as determined by (3.59), (3.61) and (3.62) with above presented parameters are shown in Fig. 3.9-3.11.

Finally, we will investigate how well the approximation for $a_{w+,out}^l = a_{w-,out}^r$ in (3.57) agrees with the actual solution in (3.54) or (3.56). To do this the absolute value of the error Δ , i.e. the difference between

$$\Delta = \left| a_{w+,out}^l - e^{i\delta} \left(1 + \frac{b^2}{\tilde{d}} \left(i \Delta p - \left(\varepsilon + \frac{b^2}{2} \right) \right) \right) \right| \quad (3.69)$$

or equivalently

$$\Delta = \left| a_{w-,out}^r - e^{i\delta} \left(1 + \frac{b^2}{\tilde{d}} \left(i \Delta p - \left(\varepsilon + \frac{b^2}{2} \right) \right) \right) \right|, \quad (3.70)$$

is depicted in Fig. 3.12 and clearly shows that the error is negligible. A similar figure can also be made for all the other amplitudes.

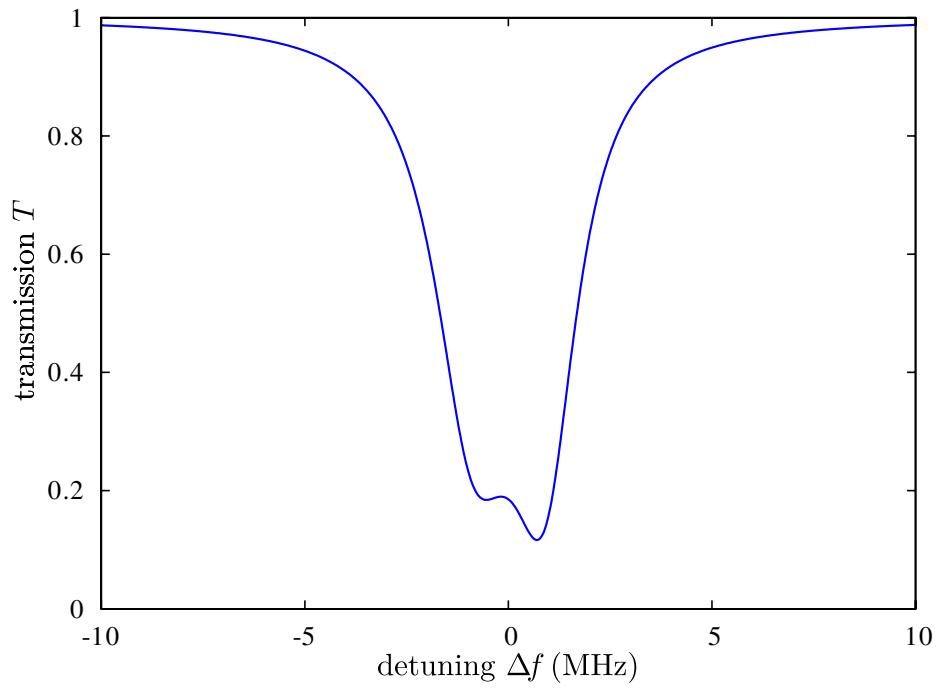


Figure 3.9: Transmission spectrum for above parameters. The spectrum is independent of the direction in which the light is injected into the fiber.

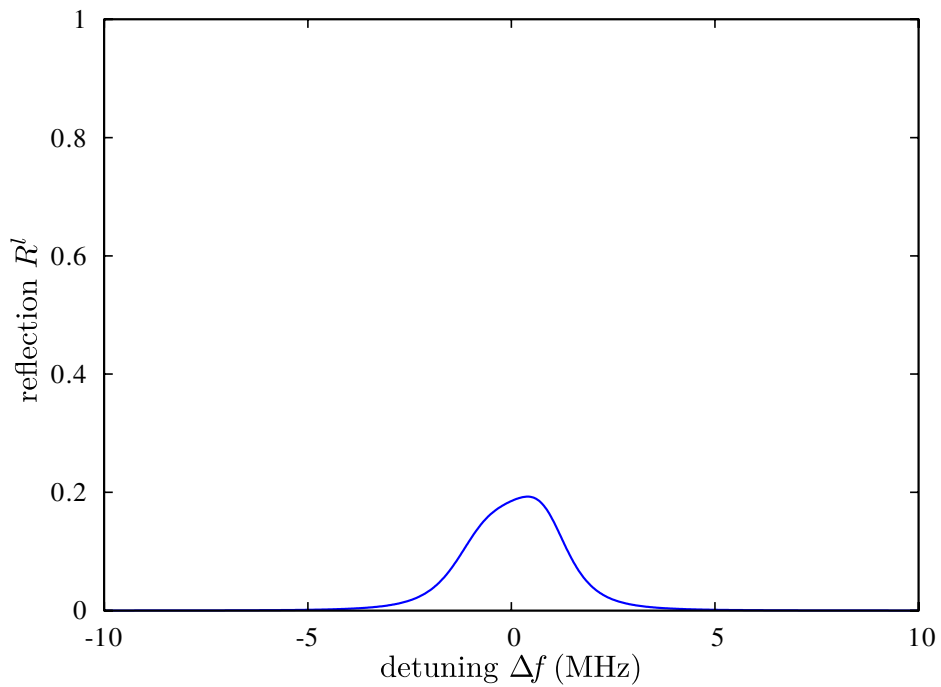


Figure 3.10: Reflection spectrum when the light is injected from the left side.

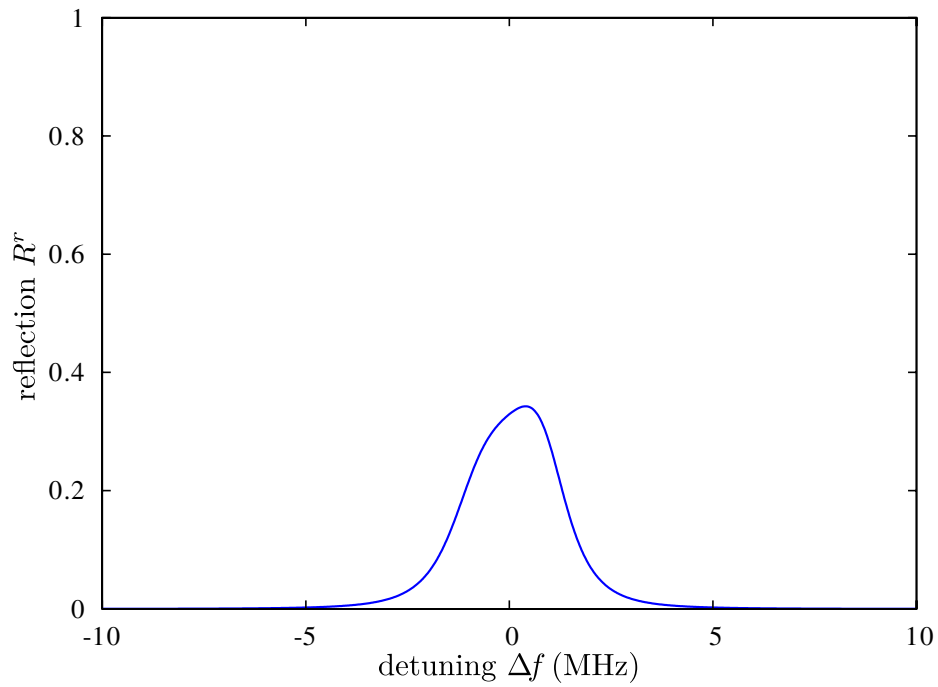


Figure 3.11: Reflection spectrum when the light is injected from the right side.

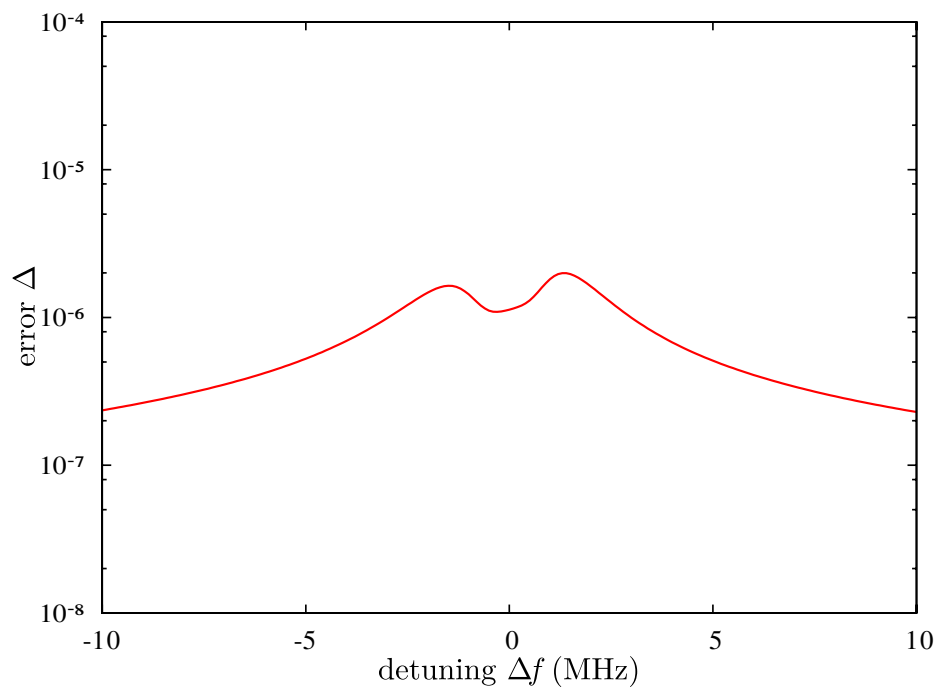


Figure 3.12: Absolute value of the error between the approximation for $a_{w+,out}^l = a_{w-,out}^r$ and its actual solution.

4 Non-Hermitian Hamiltonian Model

In this chapter we will make use of a model that has first been introduced in reference [4] and was later also used in references [5, 6]. This will lead us to model the interaction between the CW- and CCW-mode of the bottle resonator with a non-hermitian Hamiltonian. In the following we will thus refer to this model as the "non-hermitian Hamiltonian model".

In contrast to the four-mode model which treats the excitation of the modes as a stationary problem, the non-hermitian Hamiltonian model can also be used to describe dynamical features, i.e. the mode amplitudes may now vary in time. Moreover, an interesting feature of the model employed here is that it gives rise to so-called "chiral modes"¹⁸ which were one of the major themes in the aforementioned references. Our final goal in this chapter will be to determine which implications the occurrence of chiral modes in the bottle resonator have with respect to the predicted spectra according to the four-mode model.

In the first section we will introduce the non-hermitian Hamiltonian model and its basic concepts will be explained. Next, a connection between our previous four-mode model and the current non-hermitian Hamiltonian model will be established. There the main idea will be that both models actually describe the same system when the coupling strength of the four-mode model becomes zero. At the beginning of the last section, we will first investigate the time evolution of the bottle resonator modes as predicted by the non-hermitian Hamiltonian model. Afterwards, by demanding that no energy shall be created within the resonator, we will derive a condition for the model parameters which can be shown to be equivalent to (3.51) from the previous four-mode model deduced earlier. Finally, from this condition, a relationship between the so-called "chirality" and "frequency splitting quality" can be derived, which has been qualitatively discussed in reference [6].

4.1 Introduction

The above mentioned papers, i.e. [4–6], investigated the properties of the modes in the spiral-shaped cavity, the asymmetric limaçon cavity and a microdisk perturbed

¹⁸ A precise definition will be given later on.

by two nanoparticles which are all open systems just like the bottle resonator. Note that, due to the deformed boundaries of these systems (or the perturbation of nanoparticles), the rotational and the left-right symmetry¹⁹ is broken, in contrast to a perfect bottle resonator. Here "deformed" is to be understood in relation to a perfectly circular shaped cavity whose modes we will refer to as the "unperturbed" ones.

In all of the three above mentioned resonators almost degenerate mode pairs were found, for which case both modes almost have the same (complex) eigenfrequency. One might expect that one mode of such a pair could be classified as a CW-rotating mode and the other one as a CCW-rotating mode. However, the above references reported that this is in general not possible and that both modes often exhibited the same preferred sense of rotation, be it CW or CCW. The modes of such a mode pair were named "chiral modes" and such a property "chirality".²⁰ Moreover, it has also been shown that the modes of such an almost degenerate pair were nearly collinear when both modes had the same preferred sense of rotation. On the contrary, since the unperturbed modes are exactly degenerate, they can always be chosen to be a pair of CW- and CCW-propagating modes. The non-Hermitian Hamiltonian model, which was first introduced in [4] and was further used in [5, 6], successfully linked above findings to asymmetric scattering between the CW- and CCW-propagating modes.

In the following the two-mode approximation will be used, i.e. the optical field will be approximated as a superposition of the two degenerate unperturbed CW- and CCW-mode whose eigenfrequency is in close proximity to the ones of the almost degenerate mode pair of interest. By additionally employing the slowly varying envelope approximation Maxwell's equations can be reformulated as a Schrödinger-like equation, i.e.

$$i \partial_t \vec{\psi}(t) = H \vec{\psi}(t) \quad \text{with} \quad \vec{\psi}(t) = \begin{pmatrix} \psi_+ \\ \psi_- \end{pmatrix} \quad (4.1)$$

where ψ_+ (ψ_-) denotes the amplitude of the CCW-mode (CW-mode). In other words, the basis vectors $(1, 0)^T$ and $(0, 1)^T$ correspond to the CCW-mode and the CW-mode, respectively.

Due to the openness of the system the Hamiltonian H in references [4–6] was modelled as non-hermitian, i.e.

$$H = H_0 + H_1 \quad (4.2)$$

$$\text{with} \quad H_0 = \begin{pmatrix} \omega_0 & 0 \\ 0 & \omega_0 \end{pmatrix} \quad \text{and} \quad H_1 = \begin{pmatrix} \Gamma & V \\ \eta V^* & \Gamma \end{pmatrix}$$

¹⁹ This may also be called mirror symmetry.

²⁰ not to be confused with the optical activity in chiral media

$$\text{where } V = |V| e^{i\nu} \quad \text{and} \quad \Gamma = \Gamma_r + i\Gamma_i.$$

The first part of the Hamiltonian H_0 describes the situation for the circular shaped cavity, where ω_0 is a real number and denotes the eigenfrequency of the unperturbed degenerate mode pair. The second part of the Hamiltonian H_1 accounts for the interaction between the CW- and CCW-mode caused by the deformed boundaries (or the nanoparticles).

The parameter Γ shall in general be a complex number, where its real part Γ_r apparently just shifts the resonance frequency ω_0 and its imaginary part Γ_i gives rise to an exponential decay of the mode amplitudes. Furthermore, V and η shall also be complex numbers and the phase ν can obviously be chosen to lie within the range of $[-\pi, \pi]$. After looking at (4.1) and (4.2) it is clear that the off-diagonal element V (ηV^*) describes the scattering from the CW-mode (CCW-mode) to the CCW-mode (CW-mode). Consequently, the absolute value of V is a measure for the scattering strength between the counterpropagating modes and $|\eta|$ measures the asymmetry of their scattering to one another.

In the following we will assume that the scattering from the CW-mode to the CCW-mode shall be stronger than the other way around which can equivalently be expressed by

$$0 \leq |\eta| \leq 1. \quad (4.3)$$

Having said that, if it were the case that the CW-mode would scatter stronger into the CCW-mode than vice versa we could just swap ψ_+ and ψ_- in the definition of $\vec{\psi}$ in (4.1). This would effectively exchange the meaning of above mentioned basis vectors with respect to the modes. Hence, the condition for η in (4.3) would still be valid and the representation for H_1 , or even H , in (4.2) would not have changed.²¹

4.2 Connection to Four-Mode Model

In this section our aim is to establish a connection between the four-mode model from the previous chapter and the current non-hermitian Hamiltonian model. In order to do this the eigenmodes and -frequencies of both models will be compared where a vanishing coupling strength will be assumed for the four-mode model to describe the same system as the non-hermitian Hamiltonian model.

Note that we have so far only discussed the modes of the cavities as treated in the papers [4–6]. However, any considerations we made in 4.1 can directly be adopted to the case of the bottle resonator. Our so-called unperturbed CW- and CCW-modes from before correspond directly to a pair of CW- and CCW-propagating bottle resonator modes. Like previously, the first part of the Hamiltonian H_0 in (4.2) would suffice to adequately describe the bottle resonator without any form of deformation or perturbation. However, surface roughness or any other imperfection

²¹ Although the basis in which the Hamiltonian is written would have changed.

of the resonator due to the limited precision of the manufacturing process may give rise to a non-zero second part of the Hamiltonian, i.e. H_1 .

4.2.1 Eigenmodes of the Non-Hermitian Hamiltonian and the Four-Mode Model

Eigenmodes according to the Non-Hermitian Hamiltonian Model

Let us first investigate the eigenfrequencies and their respective eigenmodes as predicted by the non-hermitian Hamiltonian model. Looking at (4.1) and (4.2) it is clear that the eigenmodes are given by

$$\vec{\psi}_1 = \frac{1}{\sqrt{1+|\eta|}} \begin{pmatrix} 1 \\ \sqrt{\eta} e^{-i\nu} \end{pmatrix} \quad \text{and} \quad \vec{\psi}_2 = \frac{1}{\sqrt{1+|\eta|}} \begin{pmatrix} 1 \\ -\sqrt{\eta} e^{-i\nu} \end{pmatrix} \quad (4.4)$$

with their respective eigenfrequencies

$$\omega_1 = \omega_0 + \Delta\omega_1 \quad \text{and} \quad \omega_2 = \omega_0 + \Delta\omega_2 \quad (4.5)$$

$$\text{with} \quad \Delta\omega_1 = \Gamma + \sqrt{\eta}|V| \quad \text{and} \quad \Delta\omega_2 = \Gamma - \sqrt{\eta}|V|$$

where the vectors in (4.4) are already normalized. Therefore the time dependence of the two modes must be given by $e^{i\omega_1 t}$ and $e^{i\omega_2 t}$, respectively. As we have already mentioned earlier, the model parameter Γ_r just shifts the resonance frequency of the whole system as is evident when looking at (4.5).

Eigenmodes according to the Four-Mode Model

Next, we will deal with the four-mode model where we will set one of its parameters, namely the coupling strength b , to zero. This effectively removes the waveguide from the system since its modes can now no longer interact with those of the resonator. As has already been mentioned earlier, the four-mode model then describes the same problem as the non-hermitian Hamiltonian model illustrated in Fig. 4.1.

Consequently, the only "essential" equations that remain are

$$\vec{b}_{out} = S_s \vec{b}_{in} \quad (4.6)$$

$$\text{with} \quad \vec{b}_{in} = \begin{pmatrix} b_{r+,in} \\ b_{r-,in} \end{pmatrix} \quad \text{and} \quad \vec{b}_{out} = \begin{pmatrix} b_{r-,out} \\ b_{r+,out} \end{pmatrix},$$

as we remember from (3.44), and

$$b_{r+,in} = b_{r+,out} e^{i \frac{2\pi\Delta f}{\text{FSR}_m}} \quad \text{and} \quad b_{r-,in} = b_{r-,out} e^{i \frac{2\pi\Delta f}{\text{FSR}_m}}, \quad (4.7)$$

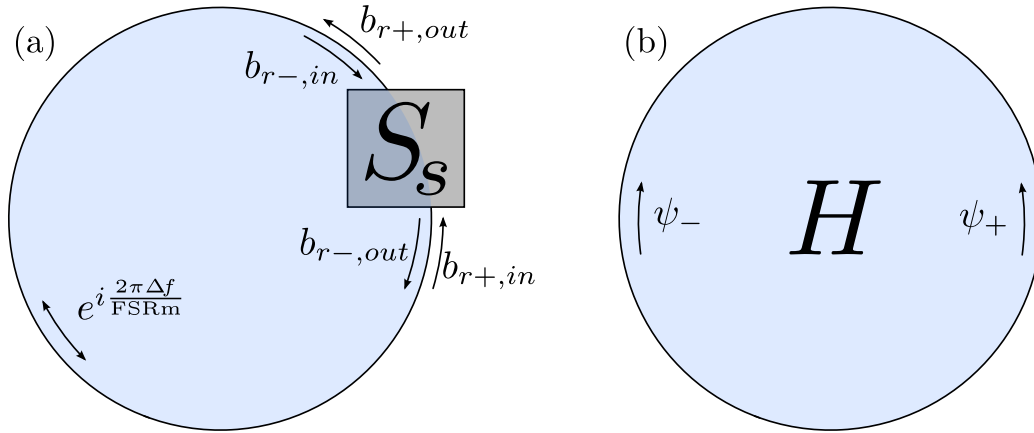


Figure 4.1: Block diagram to illustrate how the four-mode model (a) is connected with the non-hermitian Hamiltonian model (b). Note that, for a vanishing coupling strength b , the fiber in the four-mode model is no longer present (compare (a) with Fig. 3.8) and actually describes the same system as the non-hermitian Hamiltonian model.

which can be derived from (3.38), (3.52) and (3.53) when b equals zero. Moreover, we can rewrite (4.6) and (4.7) as

$$\sigma_x S_s \begin{pmatrix} b_{r+,in} \\ b_{r-,in} \end{pmatrix} = e^{-i \frac{2\pi \Delta f}{\text{FSR}_m}} \begin{pmatrix} b_{r+,in} \\ b_{r-,in} \end{pmatrix} \quad (4.8)$$

where we made use of the Pauli matrix

$$\sigma_x = \begin{pmatrix} 0 & 1 \\ 1 & 0 \end{pmatrix}.$$

Equation (4.8) is basically an eigenvalue problem and the eigenvectors of the matrix $\sigma_x S_s$ are just the eigenmodes of the bottle resonator.

4.2.2 Linking Both Models

As has already been mentioned, setting the coupling strength b in the four-mode model equal zero effectively removes the waveguide from the system. Hence, it then, like the non-hermitian Hamiltonian model, only describes the bottle resonator. Because it cannot make any difference how we calculate the resonator's eigenmodes, both models need to yield the same result. Due to the same reason we further stipulate that the resonance frequencies as predicted from both models must also comply with each other. Consequently, if the eigenfrequencies according to the non-hermitian Hamiltonian model are given by $\Delta\omega_1$ and $\Delta\omega_2$, it then follows from

the four-mode model that the eigenvalues of the matrix $\sigma_x S_s$ must be given by $e^{-i\frac{\Delta\omega_1}{\text{FSRm}}}$ and $e^{-i\frac{\Delta\omega_2}{\text{FSRm}}}$, cf. (4.8).

Therefore comparing the diagonalization of aforementioned matrix according to the just mentioned eigenmodes and -values with its representation as given by (3.46) yields

$$\begin{aligned} \sigma_x S_s &= e^{i\theta} \begin{pmatrix} 1 - \varepsilon & i r_m \\ i r_p & 1 - \varepsilon \end{pmatrix} = \\ &= \frac{1}{2} \begin{pmatrix} s_1 + s_2 & (s_1 - s_2)\frac{e^{i\nu}}{\sqrt{\eta}} \\ (s_1 - s_2)\frac{\sqrt{\eta}}{e^{i\nu}} & s_1 + s_2 \end{pmatrix} = X D X^{-1} \end{aligned} \quad (4.9)$$

where we used the abbreviations

$$X = (\psi_1, \psi_2) = \frac{1}{\sqrt{1 + |\eta|}} \begin{pmatrix} 1 & 1 \\ \sqrt{\eta} e^{-i\nu} & -\sqrt{\eta} e^{-i\nu} \end{pmatrix} \quad (4.10)$$

$$\text{and } D = \begin{pmatrix} s_1 & 0 \\ 0 & s_2 \end{pmatrix} \quad \text{with } s_1 = e^{-i\frac{\Delta\omega_1}{\text{FSRm}}} \quad \text{and } s_2 = e^{-i\frac{\Delta\omega_2}{\text{FSRm}}}.$$

Note that the model parameters Γ_i and $|V|$ shall be small compared to the free spectral range FSRm since they respectively correspond to dissipation and reflection in the bottle resonator. As mentioned earlier, the resonators are supposed to have a high quality factor. In contrast to the dissipation and backscattering we will not assume that the parameter Γ_r , which just shifts the resonance frequency, shall be small. Therefore the expressions $e^{-i(i\Gamma_i + \sqrt{\eta}|V|)}$ and $e^{-i(i\Gamma_i - \sqrt{\eta}|V|)}$, which occur when inserting (4.5) for $\Delta\omega_1$ and $\Delta\omega_2$ in (4.10), can be well approximated by their Taylor expansion in Γ_i and $|V|$ of the first order. Finally, evaluating the equality (4.9) for each matrix entry separately results in

$$\begin{aligned} \theta &= -\frac{\Gamma_r}{\text{FSRm}} \\ \varepsilon &\approx -\frac{\Gamma_i}{\text{FSRm}} \\ r_p &\approx -\frac{\eta V^*}{\text{FSRm}} \\ r_m &\approx -\frac{V}{\text{FSRm}} \end{aligned} \quad (4.11)$$

which associates the parameters of the four-mode model with the ones of the non-hermitian Hamiltonian model. Furthermore, equation (4.11) nicely complies with the fact that r_p (r_m) and ηV^* (V) both describe the scattering from the CCW- (CW-) to the CW-mode (CCW-mode).

4.3 No Energy Creation

In contrast to the four-mode model where we have studied a static problem, namely the occupation of the modes when light is constantly injected with a given driving frequency, we can now, with the help of the non-hermitian Hamiltonian model, investigate the dynamics of how the excitation of the bottle resonator modes varies with time for any given initial condition. In the following we are going to show how the CW- and CCW-mode amplitudes evolve in time according to (4.1) and (4.2) and will deduce a condition for our model parameters Γ_i , V and η which ensures that the energy in the system can only decrease or remain constant but never increase.

4.3.1 Time Evolution

In order to simplify the Schrödinger-like equation in (4.1) one can define

$$\vec{\psi}' = \begin{pmatrix} \psi'_+ \\ \psi'_- \end{pmatrix} = e^{-i\omega_0 t} \begin{pmatrix} \psi_+ \\ \psi_- \end{pmatrix} = e^{-i\omega_0 t} \vec{\psi}. \quad (4.12)$$

Inserting this into (4.1) then results in

$$i \partial_t \vec{\psi}' = H_1 \vec{\psi}'. \quad (4.13)$$

The newly introduced expressions ψ'_+ and ψ'_- in the equation above are just the mode amplitudes where the time dependence of $e^{-i\omega_0 t}$ is implicitly assumed.

Since we already know the eigenvectors of H (and thus H_1) the solution of (4.13) is simply given by

$$\vec{\psi}' = A_1 e^{i\Delta\omega_1 t} \psi_1 + A_2 e^{i\Delta\omega_2 t} \psi_2 \quad (4.14)$$

where the constants A_1 and A_2 are in general complex numbers and just represent the amplitudes of the resonator's eigenmodes. These two amplitudes must be determined through a given initial condition, which can generally be written as

$$\vec{\psi}(t=0) = \vec{\psi}'(t=0) = \begin{pmatrix} A_+ \\ A_- \end{pmatrix} \quad (4.15)$$

where A_+ and A_- can also in general be complex numbers and shall denote the initial occupation of the CW- and CCW-modes, respectively. Because the expression in (4.14) has to coincide with the one in (4.15) for $t=0$ we obtain

$$\frac{A_1}{\sqrt{1+|\eta|}} \begin{pmatrix} 1 \\ \sqrt{\eta} e^{-i\nu} \end{pmatrix} + \frac{A_2}{\sqrt{1+|\eta|}} \begin{pmatrix} 1 \\ -\sqrt{\eta} e^{-i\nu} \end{pmatrix} = \begin{pmatrix} A_+ \\ A_- \end{pmatrix} \quad (4.16)$$

or equivalently

$$\begin{aligned}\tilde{A}_1 &= \frac{A_+ + A_- \frac{e^{i\nu}}{\sqrt{\eta}}}{2} \\ \tilde{A}_2 &= \frac{A_+ - A_- \frac{e^{i\nu}}{\sqrt{\eta}}}{2}\end{aligned}\tag{4.17}$$

$$\text{with } \tilde{A}_1 = \frac{A_1}{\sqrt{1+|\eta|}} \quad \text{and} \quad \tilde{A}_2 = \frac{A_2}{\sqrt{1+|\eta|}}$$

which just translates the initial amplitudes of the CW- and CCW-modes into the amplitudes of the two eigenmodes of the resonator.

4.3.2 Condition for Model Parameters

Like for the four-mode model of the previous chapter in 3.2.1 we will again demand that no energy may be created inside the bottle resonator. Therefore the overall energy from the CW- and CCW-mode, which is proportional to

$$\|\vec{\psi}(t)\|^2 = |\psi_+|^2 + |\psi_-|^2,\tag{4.18}$$

may only decrease or remain constant but not increase, i.e.

$$\partial_t \|\vec{\psi}(t)\|^2 \leq 0.\tag{4.19}$$

It is important to note that the above inequality does not only need to be valid for all times t , but must also be satisfied regardless of the initial condition, i.e. A_+ and A_- , or equivalently for arbitrary A_1 and A_2 , cf. (4.17).

First, let us derive an explicit formula for $\|\vec{\psi}(t)\|^2$ in (4.14) via inserting the previously derived time evolution for ψ_+ and ψ_- from equation (4.18) which, after doing some formula manipulation, yields

$$\begin{aligned}\|\vec{\psi}(t)\|^2 &= \left((1+|\eta|) \left(|\tilde{A}_1|^2 e^{2\text{Im}(\sqrt{\eta})|V|t} + |\tilde{A}_2|^2 e^{-2\text{Im}(\sqrt{\eta})|V|t} \right) + \right. \\ &\quad \left. + 2|\tilde{A}_1||\tilde{A}_2|(1-|\eta|) \cos(2\text{Re}(\sqrt{\eta})|V|t + \alpha) \right) e^{2\Gamma_i t}\end{aligned}\tag{4.20}$$

where we newly introduced the abbreviation

$$\alpha = \text{Arg}(\tilde{A}_1) - \text{Arg}(\tilde{A}_2).\tag{4.21}$$

After subsequently calculating the time derivative of above expression, which we need in (4.19), and reshuffling a couple of terms one obtains

$$\begin{aligned} \partial_t \|\vec{\psi}(t)\|^2 &= 2 \left((1 + |\eta|) \left(|\tilde{A}_1|^2 (\Gamma_i + \lambda) e^{2\lambda t} + |\tilde{A}_2|^2 (\Gamma_i - \lambda) e^{-2\lambda t} \right) + \right. \\ &\quad \left. + 2 |\tilde{A}_1| |\tilde{A}_2| (1 - |\eta|) \left(\Gamma_i \cos(2\kappa t - \alpha) - \kappa \sin(2\kappa t - \alpha) \right) \right) e^{2\Gamma_i t} \end{aligned} \quad (4.22)$$

where we again introduced new abbreviations, i.e.

$$\kappa = \text{Re}(\sqrt{\eta}) |V| \quad \text{and} \quad \lambda = \text{Im}(\sqrt{\eta}) |V|. \quad (4.23)$$

With the above derived expression (4.22) we can now rewrite (4.19) as

$$\begin{aligned} (1 + |\eta|) \left(|\tilde{A}_1|^2 (\Gamma_i + \lambda) e^{2\lambda t} + |\tilde{A}_2|^2 (\Gamma_i - \lambda) e^{-2\lambda t} \right) + \\ + 2 |\tilde{A}_1| |\tilde{A}_2| (1 - |\eta|) \left(\Gamma_i \cos(2\kappa t - \alpha) - \kappa \sin(2\kappa t - \alpha) \right) \leq 0 \end{aligned} \quad (4.24)$$

where we omitted the factor $2e^{2\Gamma_i t}$ because it can only take positive values and therefore doesn't affect the validity of the inequality.

Since it is important for the following consideration, let us again emphasize that the inequality in (4.19), and thus (4.24), does not only need to hold for all times t but also for any initial condition and hence for arbitrary A_1 and A_2 . Consequently, we need to find the least upper bound, i.e. the supremum,²² for the left hand side in (4.24), which just represents the worst case for which said inequality must still be fulfilled.

First, let us investigate the first term in (4.24), i.e.

$$|\tilde{A}_1|^2 (\Gamma_i + \lambda) e^{2\lambda t} + |\tilde{A}_2|^2 (\Gamma_i - \lambda) e^{-2\lambda t}, \quad (4.25)$$

where we omitted the factor $(1 - |\eta|)$ since it will be no importance. From the above expression it is quite clear that the dissipation Γ_i has to obey

$$\Gamma_i + \lambda < 0 \quad \text{and} \quad \Gamma_i - \lambda < 0 \quad (4.26)$$

since otherwise $\partial_t \|\vec{\psi}(t)\|^2$ could get arbitrarily large, e.g. if $\Gamma_i + \lambda$ would be greater than zero this could simply be accomplished by setting $A_2 = 0$ and letting A_1 go to infinity.²³ Also note that the conditions in (4.26) imply that Γ_i must always be smaller than zero. With the previous considerations in mind we now know that (4.25) is strictly positive and calculating its supremum is quite an easy task since it is a standard problem in analysis and results in

$$-2 |\tilde{A}_1| |\tilde{A}_2| \sqrt{\Gamma_i^2 - \lambda^2}. \quad (4.27)$$

²² Since the supremum can be reached it is also a maximum.

²³ If $\Gamma_i - \lambda > 0$ would be the case the roles of A_1 and A_2 need to be reversed.

Next, we will take a closer look at the second term in (4.24), i.e.

$$\Gamma_i \cos(2\kappa t - \alpha) - \kappa \sin(2\kappa t - \alpha), \quad (4.28)$$

where we again omitted all unimportant prefactors. Be aware that we have already fixed ourselves to a certain point in time to maximize (4.25). Fortunately, this won't be a problem since the least upper bound of above expression can always be reached, that is to say, independently of t by just setting the phase

$$\alpha = 2\kappa t - \alpha_0 \quad (4.29)$$

with α_0 denoting the value of α where (4.28) takes on its maximum for $t = 0$. Therefore by just making use of standard trigonometric identities we obtain

$$\sqrt{\Gamma_i^2 + \kappa^2} \quad (4.30)$$

for the supremum of aforementioned expression.

Consequently, due to the results from (4.27) and (4.30), we can conclude that the least upper bound of the left hand side of (4.24) is just given by

$$2 |\tilde{A}_1| |\tilde{A}_2| \left(- (1 + |\eta|) \sqrt{\Gamma_i^2 - \lambda^2} + (1 - |\eta|) \sqrt{\Gamma_i^2 + \kappa^2} \right) \quad (4.31)$$

and since the condition in (4.24) must still be satisfied for (4.31) we can therefore rewrite it as

$$(1 - |\eta|) \sqrt{\Gamma_i^2 + \kappa^2} \leq (1 + |\eta|) \sqrt{\Gamma_i^2 - \lambda^2}. \quad (4.32)$$

After squaring both sides of above inequality (which we can do since they are both positive), inserting the definitions for ε and δ , cf. (4.23), and subsequently rearranging some terms one obtains

$$|\eta| \left(1 + 2 (\text{Im}(\sqrt{\eta})^2 - \text{Re}(\sqrt{\eta})^2) + |\eta|^2 \right) |V|^2 \leq 4 |\eta| \Gamma_i^2 \quad (4.33)$$

Furthermore, making use of the identity

$$|1 - \eta|^2 = 1 + 2 (\text{Im}(\sqrt{\eta})^2 - \text{Re}(\sqrt{\eta})^2) + |\eta|^2, \quad (4.34)$$

taking the square root of (4.33) and solving for $-\Gamma_i$ finally yields²⁴

$$-\Gamma_i \geq \frac{|1 - \eta|}{2} |V| \quad (4.35)$$

which is nicely in accordance to (3.51) when the parameters of the four-mode model are replaced by their counterparts of the non-hermitian Hamiltonian model, cf. (4.11).

²⁴ Note that $-\Gamma_i$ is a positive number.

4.3.3 Chirality and Frequency Splitting Quality

In the references [5, 6] two quantities, namely the so-called "frequency splitting quality" defined as

$$Q_{sp} := \frac{\operatorname{Re}(\omega_1) - \operatorname{Re}(\omega_2)}{-\operatorname{Im}(\omega_1) - \operatorname{Im}(\omega_2)} \quad (4.36)$$

and the so-called "chirality" defined as²⁵

$$\alpha := 1 - |\eta|, \quad (4.37)$$

were introduced. From above definitions one can see that Q_{sp} is a measure for the resonance frequency splitting in a spectrum in terms of the linewidth and that α measures the imbalance between the occupation of the CW- and CCW-mode in the resonator's eigenmodes, cf. (4.4). In the following we will derive a condition which the frequency splitting quality and the chirality ought to fulfil according to the non-hermitian Hamiltonian model.

At first let us insert the expressions from (4.5) for ω_1 and ω_2 into (4.36) which results in

$$Q_{sp} = |\operatorname{Re}(\sqrt{\eta})| \frac{|V|}{(-\Gamma_i)}. \quad (4.38)$$

With the help of (4.38), one can then rewrite (4.35) as

$$1 \geq \frac{|1 - \eta|}{|\operatorname{Re}(\sqrt{\eta})|} \frac{Q_{sp}}{2}. \quad (4.39)$$

Furthermore, using that

$$\frac{|1 - \eta|}{|\operatorname{Re}(\sqrt{\eta})|} \geq \frac{1 - |\eta|}{\sqrt{|\eta|}} = \frac{\alpha}{\sqrt{1 - \alpha}}, \quad (4.40)$$

where the right hand side of the inequality is just the minimum of the left hand side, one can deduce the condition

$$1 \geq \frac{\alpha}{\sqrt{1 - \alpha}} \frac{Q_{sp}}{2}, \quad (4.41)$$

which must be fulfilled by α and Q_{sp} . Finally, squaring (4.41), which is allowed since both sides are positive, and doing some rearranging of terms one obtains

$$0 \geq \frac{Q_{sp}^2}{4} \alpha^2 + \alpha - 1 = (\alpha - \alpha_1)(\alpha - \alpha_2) \quad (4.42)$$

$$\text{with } \alpha_1 = \frac{-1 - \sqrt{1 + Q_{sp}^2}}{Q_{sp}^2/2} \quad \text{and} \quad \alpha_2 = \frac{-1 + \sqrt{1 + Q_{sp}^2}}{Q_{sp}^2/2}$$

²⁵ The definition would actually be $\alpha := 1 - \min(|\eta|, \frac{1}{|\eta|})$ if (4.3) had not be stipulated.

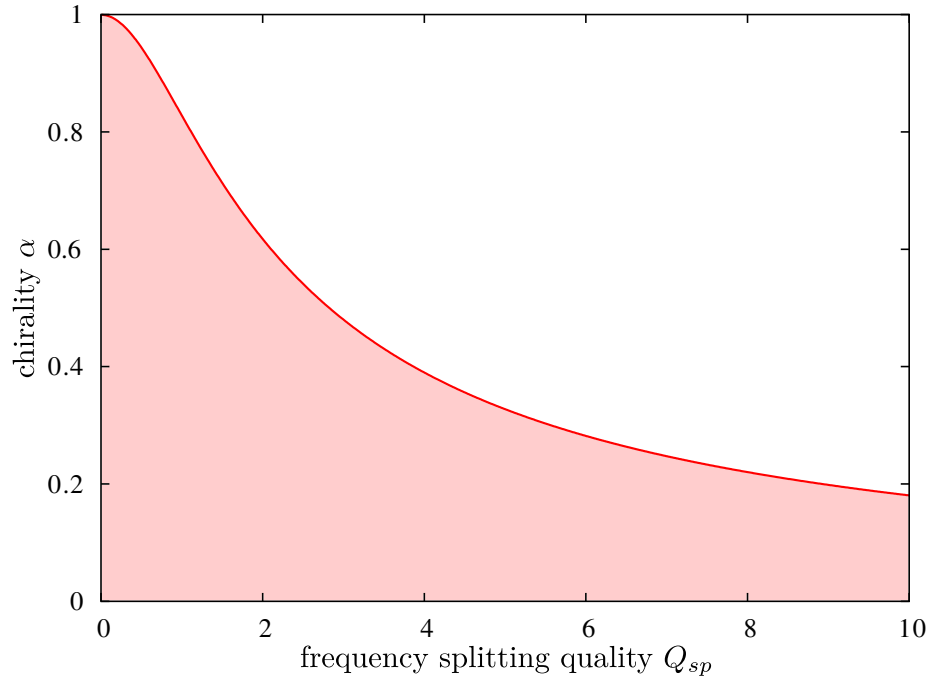


Figure 4.2: The bright red area under the red line indicates the allowed values for the chirality α and the frequency splitting quality Q_{sp} . Ultimately this constraint for both quantities has been derived from the postulation that no energy shall be created inside the resonator.

or equivalently

$$0 \leq \alpha \leq \alpha_2 \quad (4.43)$$

where zero has been used as a lower bound instead of α_1 since the chirality cannot be negative. Note that, since we used the minimum of the left hand side in (4.40) as its lower estimation, the above inequality defines the smallest parameter space within which both α and Q_{sp} always have to lie.

The region of allowed values for the frequency splitting quality and chirality is indicated by the bright red area shown in Fig 4.2. By looking at the figure it becomes obvious that the high values for α are only possible for low values of Q_{sp} , which has already been observed in reference [6], and we have now essentially explained by the postulation that no energy shall be created inside the resonator. An elegant possibility to test the model would thus be to experimentally determine both α and Q_{sp} for different mode pairs and subsequently check if they are always located in said region.

5 Preliminary Experimental Data and Chiral Modes

In the following chapter we will investigate how the experimental data measured and provided by the group of Arno Rauschenbeutel complies with the predictions of the models described in the previous chapters. In particular we will be interested to show if the effects of chiral modes, which are allowed to occur in the non-hermitian Hamiltonian model, can be observed in actual experiments.

5.1 Transmission and Reflection

First, let us discuss the experimental set-up shown in Fig. 5.1 which is quite similar to the one depicted in Fig. 3.8. The main difference is that instead of one fiber, two are used, where the purpose of the upper one is to bring the laser light into the system and the lower one is utilized to measure the transmission and reflection spectra. For the measurement of the spectra, shown in Fig. 5.2, the injected light's frequency was varied around the resonance frequency of a bottle resonator mode pair. Transmission and reflection spectra were recorded for both cases when the light came from the right-hand and from the left-hand side. In the experiment the upper waveguide was located sufficiently far apart from the cavity such that its coupling strength to the resonator, which we will denote by b' , is much smaller than the one from the lower waveguide, i.e.

$$b' \ll b. \quad (5.1)$$

Therefore, the light inside the cavity will mainly leave through the lower fiber with the losses due to the upper one being negligible.

For the time being let us assume that the light, whose amplitude we will denote by $c_{w,in}$, is injected from the right as shown in Fig. 5.1(b). With this and the aforementioned approximation we can easily modify the formulas of the four-mode model where the light enters the system from the left²⁶ to describe the current situation. Of course, since there is no incoming light in the lower fiber, equation (3.34) needs to be changed to

$$a_{w+,in} = 0 \quad \text{and} \quad a_{w-,in} = 0 \quad (5.2)$$

²⁶ Do not be confused here: when the light in Fig. 5.1 comes from the right we need to modify the formulas of the four-mode model where the light is injected from the left.

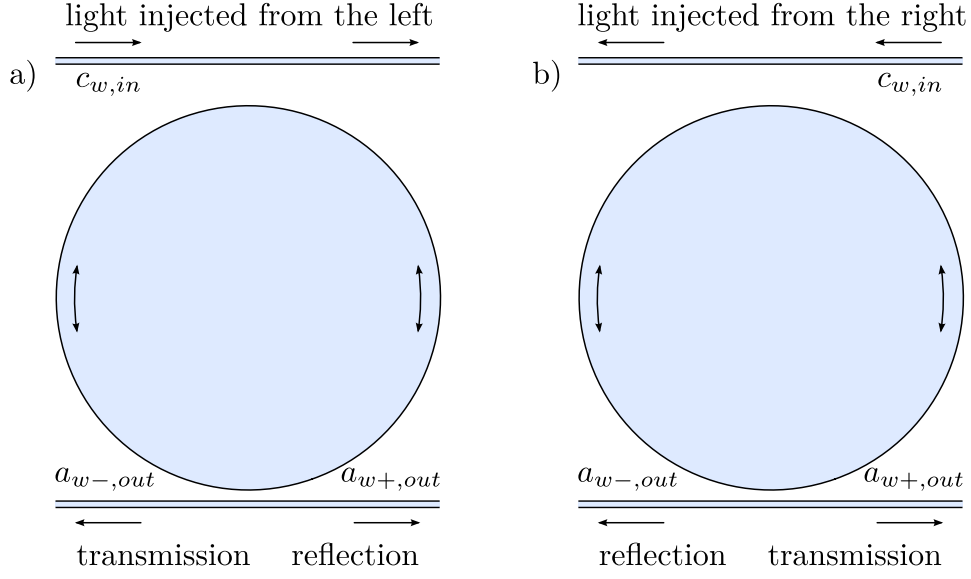


Figure 5.1: Illustration of the principal set-up of the experiment used to measure the transmission and reflection spectra shown in Fig. 5.2. The images (a) and (b) depict the two cases where the light is injected from the left- and right-hand side.

In order to account for the additional upper fiber we also need to replace the first equation in (3.52) by²⁷

$$a_{r+,out} + i b' c_{w,in} = b_{r+,in} . \quad (5.3)$$

where we made use of the approximation (5.1). All other equations of the four-mode model remain the same.

Fortunately, the solutions for this new set of equations can be obtained from the already calculated ones under 3.2.2. By simply setting

$$c_{w,in} = -b/b' \quad (5.4)$$

and defining

$$\begin{aligned} a'_{w+,in} &:= 1 \\ a'_{r+,out} &:= a_{r+,out} + i b' c_{in} \\ a'_{w+,out} &:= a_{w+,out} - i b' c_{in} \end{aligned} \quad (5.5)$$

the equations (5.3) and (3.38) can be rewritten as

$$a'_{r+,out} = b_{r+,in} \quad (5.6)$$

²⁷ For simplicity we set all phases from the four-mode model to zero here since they only change the phases of the amplitudes or the position of the resonance, cf. 3.2.2.

and

$$\vec{a}'_{out} = S_c \vec{a}'_{in} \quad \text{with} \quad (5.7)$$

$$\vec{a}'_{in} = \begin{pmatrix} a'_{r+,in} \\ a_{w+,in} \\ a_{r-,in} \\ a_{w-,in} \end{pmatrix} \quad \text{and} \quad \vec{a}'_{out} = \begin{pmatrix} a_{r-,out} \\ a_{w-,out} \\ a'_{r+,out} \\ a'_{w+,out} \end{pmatrix}.$$

Finally, comparing the above formulas with the original ones from the four-mode model shows that they actually represent the same system of equations, where the amplitudes $a_{r+,out}$, $a_{w+,in}$ and $a_{w+,out}$ are just exchanged by their primed counterparts $a'_{r+,out}$, $a'_{w+,in}$ and $a'_{w+,out}$. Therefore the amplitudes must be given by the solution already given in 3.2.2, where

$$a'_{r+,out} = a^l_{r+,out} \quad (5.8)$$

$$a'_{w+,out} = a^l_{w+,out}.$$

A similar procedure can be done when the light in the experiment is injected from the left hand side.

Due to the aforementioned considerations any predictions made about the spectra of the four-mode model should also be applicable to this experimental set-up. Looking at Fig. 5.1 one sees that the transmission spectra do, as predicted, well coincide with each other. Most interestingly the measured reflection spectra do not match which, according to the previously described non-hermitian Hamiltonian model, shows that the degenerate mode pair under investigation exhibits chirality. Although further measurements and experimental analysis may be needed to rule out other explanations for this behaviour the present result is already very promising for establishing the existence of chiral modes in (slightly perturbed) bottle resonators and encourages further investigation.

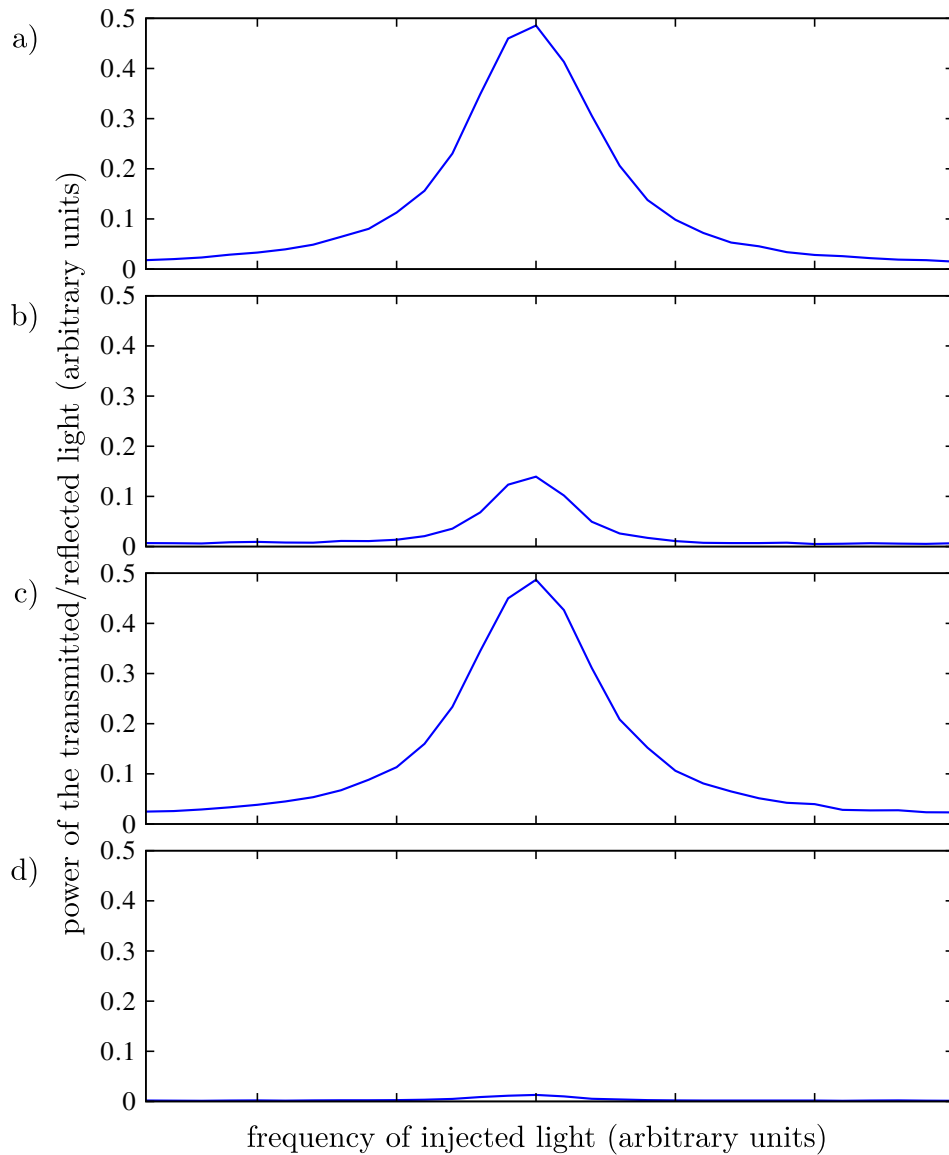


Figure 5.2: Experimentally measured transmission and reflection spectra according to the set-up depicted in Fig. 5.1 (normalized to the power of the injected light). (a) Transmission spectrum when the light comes from the left side. (b) Reflection spectrum when the light comes from the left side. (c) Transmission spectrum when the light comes from the right side. (d) Reflection spectrum when the light comes from the right side.

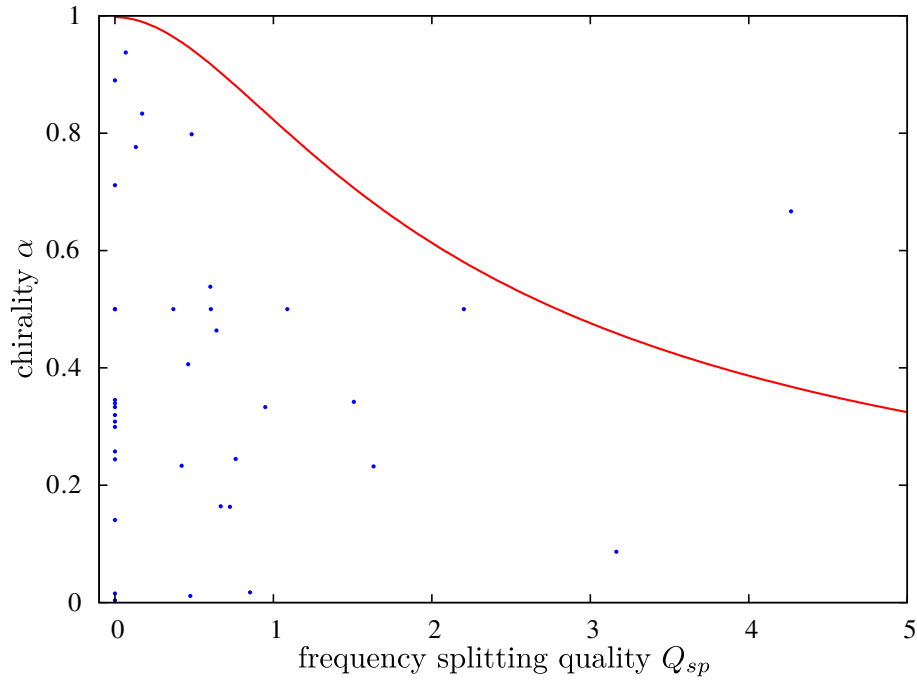


Figure 5.3: Plot showing chirality and frequency splitting quality pairs experimentally obtained for various bottle resonator modes. The red line indicates the border between allowed and forbidden values of the chirality α and the frequency splitting quality Q_{sp} .

5.2 Chirality and Frequency Splitting Quality

Next, let us discuss measurements where an experimental set-up as depicted in Fig. 3.8 was used. Again, transmission and reflection spectra have been recorded but this time not only for one but for several bottle resonator modes where for every set of parameters²⁸ a transmission spectrum and both reflection spectra were measured.²⁹ These spectra were then used to determine the respective frequency splitting quality for every such set via fitting them with a double-Lorentzian curve, cf. 3.63. Additionally, the chirality was calculated from the ratio of the reflections, cf. 3.65, 4.11 and 4.37.

²⁸ e.g. the probed mode pair, the gap between the resonator and the waveguide, etc.

²⁹ One for when the light is injected from the left and one for when the light is injected from the right.

The result of this procedure can be seen in Fig. 5.3 where a dot represents the determined chirality and frequency splitting quality of a set of parameters. As we have derived under 4.3.3 the non-hermitian Hamiltonian model predicts that these dots may only lie within the bright red area in Fig. 4.2 or, respectively, under the red line in Fig. 5.3. By looking at the figure one sees that the experimental data, with one exception, agrees well with this condition. However, for the one dot in the upper right corner in the figure further investigation revealed that random noise could have easily altered the ratio of the reflections since they were near zero. We would like to stress that this is an even more promising result than the one before to verify the occurrence of chiral modes since chirality was not only often observed to be unequal zero but also to comply with the frequency splitting quality. However, further experimental evidence may still be needed to show if there really cannot be found a single mode pair that would violate the aforementioned condition.

6 Four Dimensional Scattering Matrix for Left-Right-Symmetric Systems

In the previous four-mode model we have so far only considered coupling matrices S_c with no backscattering. However, in the course of this work a more general expression for the coupling matrix was obtained which includes reflection at the right-left symmetric coupling region. Although, no further use was made of it, it is still a nice result which shall be given an account of in this chapter. Like in the four-mode model before, we will again assume that time-reversal symmetry and energy conservation holds.

As has already been mentioned in (3.42) due to the right-left symmetry it follows that the coupling matrix S_c can be written as

$$S_c = \begin{pmatrix} A & B \\ B & A \end{pmatrix} \quad \text{with} \quad A^\top = A \quad \text{and} \quad B^\top = B \quad (6.1)$$

where A and B are 2×2 matrices and need to be symmetric in order to comply with the time reversal symmetry, cf. (3.45). The last two equations follow from the time-reversal symmetry, cf. (3.40). The ansatz for S_c in (6.1) can also be found in [24]. Additionally, from the conservation of energy, cf. (3.41), we obtain

$$A^\dagger A + B^\dagger B = I \quad \text{and} \quad A^\dagger B + B^\dagger A = 0. \quad (6.2)$$

From the singular value decomposition it follows that every matrix can be written as the product of a unitary and a positive definite hermitian matrix, i.e.

$$A = S_a H_a, \quad B = S_b H_b, \quad H_a = V_a D_a V_a^\dagger \quad \text{and} \quad H_b = V_b D_b V_b^\dagger \quad (6.3)$$

$$\text{with} \quad D_a = \begin{pmatrix} \alpha_1 & 0 \\ 0 & \alpha_2 \end{pmatrix} \quad \text{and} \quad D_b = \begin{pmatrix} \beta_1 & 0 \\ 0 & \beta_2 \end{pmatrix}$$

where S_a , S_b , V_a and V_b are unitary matrices. The constants α_1 , α_2 , β_1 , and β_2 must be positive real numbers such that H_a and H_b are positive definite hermitian matrices.

Subsequently inserting the expansions for A and B into the first equation of (6.2) yields

$$A^\dagger A + B^\dagger B = V_a D_a^2 V_a^\dagger + V_b D_b^2 V_b^\dagger = I \quad (6.4)$$

or equivalently

$$V_a^\dagger V_b D_b^2 V_b^\dagger V_a = V_c D_b^2 V_c^\dagger = I - D_a^2 \quad \text{with} \quad V_c = V_a^\dagger V_b. \quad (6.5)$$

The matrix V_c in the equation above is obviously unitary and can thus be written as

$$V_c = \begin{pmatrix} c_1 & c_2 e^{i\gamma_3} \\ -c_2 e^{-i\gamma_3} & c_1 \end{pmatrix} \begin{pmatrix} e^{i\gamma_1} & 0 \\ 0 & e^{i\gamma_2} \end{pmatrix} \quad (6.6)$$

$$\text{with} \quad c_1^2 + c_2^2 = 1, \quad c_1, c_2 \in [0, 1] \quad \text{and} \quad \gamma_1, \gamma_2, \gamma_3 \in [-\pi, \pi].$$

With this considerations in mind equation (6.5) then yields

$$\begin{aligned} V_c D_b^2 V_c^\dagger &= \begin{pmatrix} c_1 & c_2 e^{i\gamma_3} \\ -c_2 e^{-i\gamma_3} & c_1 \end{pmatrix} \begin{pmatrix} \beta_1^2 & 0 \\ 0 & \beta_2^2 \end{pmatrix} \begin{pmatrix} c_1 & -c_2 e^{i\gamma_3} \\ c_2 e^{-i\gamma_3} & c_1 \end{pmatrix} = \\ &= \begin{pmatrix} \beta_1^2 c_1^2 + \beta_2^2 c_2^2 & -c_1 c_2 e^{i\gamma_3} (\beta_1^2 - \beta_2^2) \\ -c_1 c_2 e^{-i\gamma_3} (\beta_1^2 - \beta_2^2) & \beta_2^2 c_1^2 + \beta_1^2 c_2^2 \end{pmatrix} = \begin{pmatrix} 1 - \alpha_1^2 & 0 \\ 0 & 1 - \alpha_2^2 \end{pmatrix}. \end{aligned} \quad (6.7)$$

If it were the case that $\beta_1 \neq \beta_2$ either c_1 or c_2 have to equal zero for above equation to hold. For the case $c_1 = 0$ it follows that

$$H_b = V_b D_b V_b^\dagger = V_a V_c D_b V_c^\dagger V_a^\dagger = V_a \begin{pmatrix} \beta_2 & 0 \\ 0 & \beta_1 \end{pmatrix} V_a^\dagger \quad (6.8)$$

$$\text{with} \quad V_c = \begin{pmatrix} 0 & e^{i\gamma_3} \\ -e^{-i\gamma_3} & 0 \end{pmatrix} \begin{pmatrix} e^{i\gamma_1} & 0 \\ 0 & e^{i\gamma_2} \end{pmatrix}$$

and for the case $c_2 = 0$

$$H_b = V_a \begin{pmatrix} \beta_1 & 0 \\ 0 & \beta_2 \end{pmatrix} V_a^\dagger \quad \text{with} \quad V_c = \begin{pmatrix} e^{i\gamma_1} & 0 \\ 0 & e^{i\gamma_2} \end{pmatrix}. \quad (6.9)$$

Since the phases γ_1 , γ_2 and γ_3 are obviously irrelevant for the above calculation of H_b they can simply be set to zero. Moreover, because the meaning of β_1 and β_2 is just exchanged in (6.8) compared to (6.9) we can limit ourselves to the case $c_2 = 0$. Hence we can choose that $V_b = V_a = V$ when $\beta_1 \neq \beta_2$. Trivially this is also true for $\beta_1 = \beta_2 = \beta$ because

$$H_b = V_b D_b V_b^\dagger = \beta V_b I V_b^\dagger = \beta I = \beta V_a I V_a^\dagger = V_a D_b V_a^\dagger. \quad (6.10)$$

Consequently, the first equation in (6.2) can be rewritten as

$$D_a^2 + D_b^2 = I \quad (6.11)$$

or equivalently

$$\alpha_1^2 + \beta_1^2 = 1 \quad \text{and} \quad \alpha_2^2 + \beta_2^2 = 1. \quad (6.12)$$

Furthermore, by making use of $V_b = V_a = V$ the second equation in (6.2) yields

$$D_a \bar{U} D_b + D_b \bar{U}^\dagger D_a = 0 \quad \text{with} \quad \bar{U} = V^\dagger S_a^\dagger S_b V. \quad (6.13)$$

The matrix \bar{U} is obviously unitary since it is a product of unitary matrices and can generally be represented by

$$\bar{U} = \begin{pmatrix} a e^{i\alpha} & b e^{i\beta} \\ b e^{i\gamma} & a e^{i\delta} \end{pmatrix} \quad \text{with} \quad a^2 + b^2 = 1, \quad (6.14)$$

$$e^{i(\alpha+\delta)} = -e^{i(\beta+\gamma)}, \quad a, b \in [0, 1] \quad \text{and} \quad \alpha, \beta, \gamma, \delta \in [-\pi, \pi]$$

After inserting the representation of \bar{U} into (6.13) one obtains

$$\begin{pmatrix} \alpha_1 \beta_1 a e^{i\alpha} & \alpha_1 \beta_2 b e^{i\beta} \\ \alpha_2 \beta_1 b e^{i\gamma} & \alpha_2 \beta_2 a e^{i\delta} \end{pmatrix} = - \begin{pmatrix} \alpha_1 \beta_1 a e^{-i\alpha} & \alpha_2 \beta_1 b e^{-i\gamma} \\ \alpha_1 \beta_2 b e^{-i\beta} & \alpha_2 \beta_2 a e^{-i\delta} \end{pmatrix} \quad (6.15)$$

Now two cases, i.e. $b \neq 0$ and $b = 0$, need to be distinguished. For the first case ($b \neq 0$) we get

$$\alpha_1 \beta_2 = \alpha_2 \beta_1 \quad (6.16)$$

and after making use of (6.12) and (6.14) and doing some formula manipulation one can deduce that

$$\alpha_1 = \alpha_2 = \alpha \quad \text{and} \quad \beta_1 = \beta_2 = \beta \quad \text{with} \quad \alpha^2 + \beta^2 = 1 \quad (6.17)$$

from which it follows directly, cf. (6.3), that

$$A = \alpha S_a \quad \text{and} \quad B = \beta S_b \quad (6.18)$$

$$\text{where} \quad S_b = S_a W \quad \text{with} \quad W = V \bar{U} V^\dagger$$

Inserting the ansatz for A and B into second equation (6.2) yields the condition

$$W + W^\dagger = 0 \quad (6.19)$$

where we assumed that both α and β are unequal zero.³⁰ Additionally taking into account that W is unitary since it is as a product of unitary matrices, cf. (6.19), one can show that a proper representation would be

$$W = \begin{pmatrix} \pm i a' & b' e^{i\beta'} \\ b' e^{i\beta'} & \mp i a' \end{pmatrix} \quad \text{with} \quad a'^2 + b'^2 = 1, \quad b' > 0, \quad (6.20)$$

$$a', b' \in [0, 1] \quad \text{and} \quad \beta' \in [-\pi, \pi].$$

³⁰ Otherwise one would obtain the trivial case we already employed in 3.2.1 where A (B) equals the zero matrix and B (A) must be unitary and symmetric.

Other possibilities for W would be $\pm i I$ and $\pm i \sigma_z$ but these would correspond to a \bar{U} with $b = 0$ and are thus irrelevant.³¹

For the second case ($b = 0$) we obtain

$$e^{i\alpha} = -e^{-i\alpha} = \pm i \quad \text{and} \quad e^{i\delta} = -e^{-i\delta} = \pm i \quad (6.21)$$

and inserting this into the representation of \bar{U} , i.e. (6.14), then yields

$$\bar{U} = \pm i I \quad \text{or} \quad \bar{U} = \pm i \sigma_z. \quad (6.22)$$

Finally making use of (6.3) and the second equation in (6.13) results in

$$A = U D_a V^\dagger \quad \text{with either} \quad B = \pm i U D_b V^\dagger \quad (6.23)$$

$$\text{or} \quad B = \pm i U \sigma_z D_b V^\dagger \quad \text{where} \quad U = S_a V.$$

Note that we have in (6.21) implicitly assumed that α_1 , α_2 , β_1 and β_2 are unequal zero. However, even if it were the case that one of those phases would be nil, the additional degree of freedom for \bar{U} would not yield new solutions, as can easily be shown. Thus the cases mentioned under (6.23) will suffice for our further investigation.

What remains to be done now is to take care that the time reversal symmetry, cf. (6.1), is obeyed. Let us start with the first case, cf. (6.18), for which we obtain

$$S_a^\top = S_a \quad \text{and} \quad S_b^\top = S_b \quad (6.24)$$

The unitary and symmetric matrix S_a can be chosen to be parametrized by

$$e^{i\beta_s} \begin{pmatrix} a_s e^{i\epsilon_s} & b_s \\ b_s & a_s e^{-i\epsilon_s} \end{pmatrix} \quad \text{with} \quad a_s^2 + b_s^2 = 1, \quad (6.25)$$

$$a_s, b_s \in [0, 1] \quad \text{and} \quad \beta_s, \epsilon_s \in [-\pi, \pi]$$

From the symmetry of S_b one can derive that

$$\begin{aligned} S_b &= S_a W = e^{i\beta_s} \begin{pmatrix} a_s e^{i\epsilon_s} & b_s \\ b_s & a_s e^{-i\epsilon_s} \end{pmatrix} \begin{pmatrix} \pm i a' & b' e^{i\beta'} \\ -b' e^{-i\beta'} & \mp i a' \end{pmatrix} = \\ &= e^{i\beta_s} \begin{pmatrix} \dots & \mp i a' b_s + a_s b' e^{i(\beta' + \epsilon_s)} \\ \pm i a' b_s + a_s b' e^{-i(\beta' + \epsilon_s)} & \dots \end{pmatrix} = S_b^\top \end{aligned} \quad (6.26)$$

from which it follows that

$$\pm a' b_s = a_s b' \sin(\beta' + \epsilon_s). \quad (6.27)$$

³¹ The matrix $\sigma_z = \begin{pmatrix} 1 & 0 \\ 0 & -1 \end{pmatrix}$ shall denote the Pauli matrix in the z -direction.

Equation (6.27) hence signifies which matrices W are possible for a given S_a or vice versa. The diagonal positions of the S_b matrix weren't calculated since they are irrelevant here.

Next, we are going to look at the second case, cf. (6.23), where $B = \pm iUD_bV^\dagger$. Analogous consideration need to be made for the other possibility where $B = \pm iU\sigma_z D_bV^\dagger$ which we will thus not further investigate in the following. From the time reversal symmetry it follows that

$$UD_aV^\dagger = (UD_aV^\dagger)^\top \quad \text{and} \quad UD_bV^\dagger = (UD_bV^\dagger)^\top \quad (6.28)$$

A general ansatz will be used for the two unitary matrices U , i.e.

$$U = \begin{pmatrix} a_u & b_u e^{i\beta_u} \\ -b_u e^{-i\beta_u} & a_u \end{pmatrix} \begin{pmatrix} e^{i\alpha_u} & 0 \\ 0 & e^{i\delta_u} \end{pmatrix} \quad \text{with} \quad a_u^2 + b_u^2 = 1, \quad (6.29)$$

$$a_u, b_u \in [0, 1] \quad \text{and} \quad \alpha_u, \beta_u, \delta_u \in [-\pi, \pi],$$

and V , i.e.

$$V = \begin{pmatrix} e^{i\alpha_v} & 0 \\ 0 & e^{i\delta_v} \end{pmatrix} \begin{pmatrix} a_v & b_v e^{i\beta_v} \\ -b_v e^{-i\beta_v} & a_v \end{pmatrix} \quad \text{with} \quad a_v^2 + b_v^2 = 1, \quad (6.30)$$

$$a_v, b_v \in [0, 1] \quad \text{and} \quad \alpha_v, \beta_v, \delta_v \in [-\pi, \pi].$$

Inserting above parametrization of U and V into the first equation in (6.28) yields

$$UD_aV^\dagger = \begin{pmatrix} a_u & b_u e^{i\beta_u} \\ -b_u e^{-i\beta_u} & a_u \end{pmatrix} \begin{pmatrix} \bar{\alpha}_1 & 0 \\ 0 & \bar{\alpha}_2 \end{pmatrix} \begin{pmatrix} a_v & b_v e^{i\beta_v} \\ -b_v e^{-i\beta_v} & a_v \end{pmatrix} = \quad (6.31)$$

$$= \begin{pmatrix} \dots & \bar{\alpha}_1 a_u b_v e^{i\beta_v} + \bar{\alpha}_2 a_v b_u e^{i\beta_u} \\ -\bar{\alpha}_1 a_v b_u e^{-i\beta_u} - \bar{\alpha}_2 a_u b_v e^{-i\beta_v} & \dots \end{pmatrix} = (UD_aV^\dagger)^\top$$

$$\text{with} \quad \bar{\alpha}_1 = \alpha_1 e^{i(\alpha_u - \alpha_v)} \quad \text{and} \quad \bar{\alpha}_2 = \alpha_2 e^{i(\delta_u - \delta_v)}$$

from which it follows that

$$a_u b_v (\bar{\alpha}_1 e^{i\beta_v} + \bar{\alpha}_2 e^{-i\beta_v}) + a_v b_u (\bar{\alpha}_2 e^{i\beta_u} + \bar{\alpha}_1 e^{-i\beta_u}) = 0. \quad (6.32)$$

Doing the same procedure for the second equation in (6.28) yields a similar result, namely

$$a_u b_v (\bar{\beta}_1 e^{i\beta_v} + \bar{\beta}_2 e^{-i\beta_v}) + a_v b_u (\bar{\beta}_2 e^{i\beta_u} + \bar{\beta}_1 e^{-i\beta_u}) = 0 \quad (6.33)$$

$$\text{with} \quad \bar{\beta}_1 = \beta_1 e^{i(\alpha_u - \alpha_v)} \quad \text{and} \quad \bar{\beta}_2 = \beta_2 e^{i(\delta_u - \delta_v)}.$$

By multiplying (6.32) with $\bar{\beta}_2$ and (6.33) with $\bar{\alpha}_2$ and subsequently taking the difference between both equations one can deduce that

$$(\bar{\alpha}_1 \bar{\beta}_2 - \bar{\beta}_1 \bar{\alpha}_2)(a_u b_v e^{i\beta_v} + a_v b_u e^{-i\beta_u}) = 0. \quad (6.34)$$

It is clear that (6.34) can only be fulfilled if one of its factors equals zero. For the first factor this yields

$$\bar{\alpha}_1 \bar{\beta}_2 = \bar{\beta}_1 \bar{\alpha}_2. \quad (6.35)$$

After taking the absolute value of above equation and using (6.12), it follows that

$$\alpha_1 = \alpha_2 = \alpha \quad \text{and} \quad \beta_1 = \beta_2 = \beta \quad \text{with} \quad \alpha^2 + \beta^2 = 1. \quad (6.36)$$

Subsequently, inserting (6.36) into (6.23) results in the solution

$$A = \alpha \bar{W} \quad \text{and} \quad B = \pm i \beta \bar{W} \quad \text{with} \quad \bar{W} = UV^\dagger \quad (6.37)$$

where the matrix \bar{W} is obviously unitary and needs to be symmetric due to (6.28).

On the other hand, setting the second factor in (6.34) equal zero yields

$$a_u b_v e^{i\beta_v} = -a_v b_u e^{-i\beta_u} \quad (6.38)$$

or equivalently

$$e^{i\beta_v} = -e^{-i\beta_u} \quad \text{and} \quad a_u b_v = a_v b_u \quad (6.39)$$

and from which one can further deduce that

$$a_v = a_u \quad \text{and} \quad b_v = b_u. \quad (6.40)$$

Finally, using this to calculate A and B according to (6.23) results in

$$A = \bar{W} \begin{pmatrix} \bar{\alpha}_1 & 0 \\ 0 & \bar{\alpha}_2 \end{pmatrix} \bar{W}^\top \quad \text{and} \quad B = \pm i \bar{W} \begin{pmatrix} \bar{\beta}_1 & 0 \\ 0 & \bar{\beta}_2 \end{pmatrix} \bar{W}^\top \quad (6.41)$$

$$\text{with} \quad \bar{W} = \begin{pmatrix} a_u & b_u e^{i\beta_u} \\ -b_u e^{-i\beta_u} & a_u \end{pmatrix}.$$

With this, i.e. (6.41) and (6.18) with (6.20), we have derived representations of the sub-matrices A and B of the coupling matrix S_c for a left-right symmetric coupling region that also allows for backscattering to occur. As has already been mentioned at the beginning, time reversal symmetry and energy conservation is still required to hold. Since it was assumed in the four-mode model that no reflections shall occur at the coupling region the result derived in this chapter was not further put to use in this work but may still be of interest for other applications, which is why it was reported here.

7 Summary and Outlook

Although there is currently a high interest in bottle resonators due to their advantageous properties an in-depth theoretical framework to describe their interaction with a waveguide is still missing. This thesis is dedicated to filling this gap. At the beginning of this thesis, we set up a coupled mode theory which can be used to compute the coupling of an ultra-thin fiber to a bottle resonator. We showed, in particular, how the amplitudes of the fiber and the resonator are connected through a propagation matrix, which we demonstrated to be symmetric and unitary due to energy conservation, time reversal symmetry and left-right symmetry of the coupling region. Furthermore, from the calculations done for our experimental colleagues in the group of Arno Rauschenbeutel we saw that the so-called phase matching, which itself depends on the fiber diameter, crucially influences the strength of the coupling. To recap, phase matching is achieved when the spatial phase change of the electromagnetic field of the waveguide and of the resonator mode in the propagating direction are approximately equal. One can imagine that the light coupled into the resonator at one point interferes destructively with light coupled in at another point and is therefore prevented from actually transferring energy. The main result was that by deliberately choosing a small fiber radius and thus having a poor phase matching, the resonator can be made to not disturb the light in the waveguide. This is important because it means that a conveyor belt for atoms would still be able to work near a bottle resonator. Experiments along these lines are presently in preparation.

Based on the above coupled mode theory, we developed models which rely on scattering matrices to describe transmission and reflection spectra which can be experimentally observed. While doing this we derived when critical coupling ought to occur and other quantities typically measured in experiments. Moreover, we obtained formulas which describe the shape of transmission and reflection spectra and we explained how a double Lorentzian can be constructed from these spectra. We further clarified how this can be used to extract the model parameters from actual measurements. Furthermore, we also derived a quantitative condition which the model parameters have to obey, by demanding that no energy shall be created inside the resonator. As we discussed earlier, this constraint can be used to check the validity of the model.

Intrigued by the fact that the previously described model permits different reflection spectra whether the light is injected from the left-hand or right-hand side into the fiber, we employed a model introduced in [4–6]. The most interesting feature

of this model is that it allows for chiral modes to occur whose connection to the differing reflection spectra we strived to investigate. Moreover, in contrast to the models before which viewed the amplitudes of the resonator and waveguide modes as static, this model viewed them as changing in time and could also establish a connection between the parameters of the respective models. Furthermore, by imposing that energy may only dissipate (or remain constant), we were able to derive a quantitative condition which the model parameters have to satisfy. This was one of our main findings since it could be used for proving the existence of chiral modes in the bottle resonator. Qualitatively speaking, this constraint states that chiral modes can only occur when the resonances of nearly-degenerate mode pairs overlap in the transmission or reflection spectrum.

Finally, we showed preliminary data measured in the group of Arno Rauschenbeutel which are very promising in terms of establishing the existence of chiral modes. At first, we looked at experimental transmission and reflection spectra where the reflections had different heights depending on whether the light was injected from the left-hand or right-hand side into the fiber, which would already be a sign of chiral modes. Next, the so-called chirality and the splitting of the resonances were extracted from multiple measured spectra and plotted in a diagram. The data points in the plot agreed well with the previously derived condition and thus constitute a very promising result for establishing the existence of chiral modes in bottle resonators.

Being somewhat off-topic, we deduced expressions for a general 4×4 coupling matrix which complies with energy conservation, time reversal symmetry and left-right symmetry. However, unlike in the chapters before it was not assumed that no backscattering shall occur. Although this result was derived during the course of this work it is independent of the other parts of this thesis but was still included due to its possible application to other scattering problems.

Bibliography

- [1] M. Pöllinger, D. O'Shea, F. Warken, and A. Rauschenbeutel. *Ultra-high-Q Tunable Whispering-Gallery-Mode Microresonator*. Phys. Rev. Lett. **103**, 053901 (2009).
- [2] D. O'Shea, C. Junge, M. Pöllinger, A. Vogler, and A. Rauschenbeutel. *All-optical switching and strong coupling using tunable whispering-gallery-mode microresonators*. Appl. Phys. B **105**, 129 (2011).
- [3] Y. Louyer, D. Meschede, and A. Rauschenbeutel. *Tunable whispering-gallery-mode resonators for cavity quantum electrodynamics*. Phys. Rev. A **72**, 031801 (2005).
- [4] J. Wiersig, S. W. Kim, and M. Hentschel. *Asymmetric scattering and nonorthogonal mode patterns in optical microspirals*. Phys. Rev. A **78**, 053809 (2008).
- [5] J. Wiersig, A. Eberspärcher, J.-B. Shim, J.-W. Ryu, S. Shinohara, M. Hentschel, and H. Schomerus. *Nonorthogonal pairs of copropagating optical modes in deformed microdisk cavities*. Phys. Rev. A **84**, 023845 (2011).
- [6] J. Wiersig. *Structure of whispering-gallery modes in optical microdisks perturbed by nanoparticles*. Phys. Rev. A **84**, 063828 (2011).
- [7] B. Schleder. *Coupled Mode Theory Applied to a Bottle Resonator - Waveguide System*. Projektarbeit, Vienna University of Technology (2012).
- [8] A. W. Snyder and J. D. Love. *Optical Waveguide Theory*. Chapman and Hall, London, reprint edition (1991).
- [9] D. Meschede. *Optik, Licht und Laser*. Vieweg + Teubner, Wiesbaden, 3rd edition (2008).
- [10] J. A. Buck. *Fundamentals of Optical Fibers*. Wiley, New York (1995).
- [11] F. Warken. *Ultradünne Glasfasern als Werkzeug zur Kopplung von Licht und Materie*. Doktorarbeit, University of Bonn (2007).
- [12] A. Vogler. *Kopplung zweier optischer Mikroresonatoren ultrahoher Güte über eine makroskopische Distanz*. Diplomarbeit, Mainz University (2009).

-
- [13] K. R. Hiremath, R. Stoffer, and M. Hammer. *Coupled mode theory and FDTD simulations on coupling between bend and straight optical waveguides*. In *IEEE/LEOS Benelux Chapter, Proceedings of 8'th Annual Symposium*, pp. 33–36. Enschede, The Netherlands (2003).
- [14] R. Stoffer, K. R. Hiremath, and M. Hammer. *Comparison of coupled mode theory and FDTD simulations of coupling between bent and straight optical waveguides*. In M. Bertolotti, A. Driessen, and F. Michelotti (eds.), *AIP Proceedings on Microresonators as building blocks for VLSI photonics*, volume 709 of *39th course*, pp. 366–377. International School of Quantum Electronics, Erice, Sicily (2004).
- [15] M. Hammer, K. R. Hiremath, and R. Stoffer. *Analytical approaches to the description of optical microresonator devices*. In M. Bertolotti, A. Driessen, and F. Michelotti (eds.), *AIP Proceedings on Microresonators as building blocks for VLSI photonics*, volume 709 of *39th course*, pp. 48–71. International School of Quantum Electronics, Erice, Sicily (2004).
- [16] W. P. Huang. *Coupled-mode theory for optical waveguides: an overview*. *J. Opt. Soc. Am. A* **11**, 963 (1994).
- [17] H. A. Haus and W. P. Huang. *Coupled-mode theory*. *Proceedings of the IEEE* **79**, 1505 (1991).
- [18] S. L. Chuang. *A coupled mode formulation by reciprocity and a variational principle*. *Lightwave Technology, Journal of* **5**, 5 (1987).
- [19] H. A. Haus, W. P. Huang, S. Kawakami, and N. Whitaker. *Coupled-mode theory of optical waveguides*. *Lightwave Technology, Journal of* **5**, 16 (1987).
- [20] H. A. Haus, W. P. Huang, and A. W. Snyder. *Coupled-mode formulations*. *Opt. Lett.* **14**, 1222 (1989).
- [21] A. W. Snyder, A. Ankiewicz, and A. Altintas. *Fundamental error of recent coupled mode formulations*. *Electronics Letters* **23**, 1097 (1987).
- [22] P. Schneeweiss, S. T. Dawkins, R. Mitsch, D. Reitz, E. Vetsch, and A. Rauschenbeutel. *A nanofiber-based optical conveyor belt for cold atoms*. *Appl. Phys. B* **110**, 279 (2013).
- [23] M. Cai, O. Painter, and K. J. Vahala. *Observation of Critical Coupling in a Fiber Taper to a Silica-Microsphere Whispering-Gallery Mode System*. *Phys. Rev. Lett.* **85**, 74 (2000).

-
- [24] V. A. Gopar, S. Rotter, and H. Schomerus. *Transport in chaotic quantum dots: Effects of spatial symmetries which interchange the leads*. Phys. Rev. B **73**, 165308 (2006).